

FimH Antagonists for the Oral Treatment of Urinary Tract Infections: From Design and Synthesis to in Vitro and in Vivo Evaluation

Tobias Klein,[†] Daniela Abgottspon,[†] Matthias Wittwer,[†] Said Rabbani,[†] Janno Herold,[†] Xiaohua Jiang, Simon Kleeb, Christine Lüthi, Meike Scharenberg, Jacqueline Bezençon, Erich Gubler, Lijuan Pang, Martin Smiesko, Brian Cutting, Oliver Schwardt, and Beat Ernst*

Institute of Molecular Pharmacy, Pharmacenter, University of Basel, Klingelbergstrasse 50, CH-4056 Basel, Switzerland.

[†]These authors contributed equally to the project

Received August 4, 2010

Urinary tract infection (UTI) by uropathogenic *Escherichia coli* (UPEC) is one of the most common infections, particularly affecting women. The interaction of FimH, a lectin located at the tip of bacterial pili, with high mannose structures is critical for the ability of UPEC to colonize and invade the bladder epithelium. We describe the synthesis and the in vitro/in vivo evaluation of α -D-mannosides with the ability to block the bacteria/host cell interaction. According to the pharmacokinetic properties, a prodrug approach for their evaluation in the UTI mouse model was explored. As a result, an orally available, low molecular weight FimH antagonist was identified with the potential to reduce the colony forming units (CFU) in the urine by 2 orders of magnitude and in the bladder by 4 orders of magnitude. With FimH antagonist **16b**, the great potential for the effective treatment of urinary tract infections with a new class of orally available antiinfectives could be demonstrated.

Introduction

Urinary tract infection (UTI⁴) is one of the most common infections, affecting millions of people each year. Particularly affected are women, who have a 40–50% risk to experience at least one symptomatic UTI episode at some time during their life. In addition, more than half of them experience a relapse of the infection within 6 months.^{1,2}

Although UTIs rarely cause severe diseases such as pyelonephritis or urosepsis, they are associated with high incidence rate and consume considerable healthcare resources.³ Uropathogenic *Escherichia coli* (UPEC) are the primary cause of UTIs, accounting for 70–95% of the reported cases. Symptomatic UTIs require antimicrobial treatment, often resulting in the emergence of resistant microbial flora. As a consequence, treatment of consecutive infections becomes increasingly difficult because the number of antibiotics is limited and the resistance of *E. coli* is increasing, especially in patients with diabetes, urinary tract anomaly, paraplegy, and those with permanent urinary catheter. Therefore, a new approach for the prevention and treatment of UTI with inexpensive, orally

applicable therapeutics with a low potential for resistance would have a great impact on patient care, public health care, and medical expenses.

UPEC strains express a number of well-studied virulence factors used for a successful colonization of their host.^{3–5} One important virulence factor is located on type 1 pili, allowing UPEC to adhere and invade host cells within the urinary tract. It enables UPEC to attach to oligomannosides, which are part of the glycoprotein uroplakin Ia on the urinary bladder mucosa. This initial step prevents the rapid clearance of *E. coli* from the urinary tract by the bulk flow of urine and at the same time enables the invasion of the host cells.^{3,6}

Type 1 pili are the most prevalent fimbriae encoded by UPEC, consisting of the four subunits FimA, FimF, FimG, and FimH, the latter located at the tip of the pili.⁷ As a part of the FimH subunit, a carbohydrate-recognizing domain (CRD) is responsible for bacterial interactions with the host cells within the urinary tract.⁶ The crystal structure of the FimH-CRD was solved⁸ and its complexes with *n*-butyl α -D-mannopyranoside⁹ and Man α (1–3)[Man α (1–6)]Man¹⁰ recently became available.

Previous studies showed that vaccination with FimH adhesin inhibits colonization and subsequent *E. coli* infection of the urothelium in humans.^{11,12} In addition, adherence and invasion of host cells by *E. coli* can also be prevented by α -D-mannopyranosides, which are potent antagonists of interactions mediated by type 1 pili.¹³ Whereas α -D-mannopyranosides efficiently prevent adhesion of *E. coli* to human urothelium, they are not exhibiting a selection pressure to induce antimicrobial resistance. Furthermore, environmental contamination is less problematic compared to antibiotics.¹⁴

More than two decades ago, Sharon and co-workers have investigated various mannosides and oligomannosides as

*To whom correspondence should be addressed. Phone: +41 61 267 1551. Fax: +41 61 267 1552. E-mail: beat.ernst@unibas.ch.

⁴ Abbreviations: AUC, area under the curve; Caco-2 cells, Caucasian colon adenocarcinoma cells; CFU, colony forming units; CRD, carbohydrate recognition domain; DC-SIGN, dendritic cell-specific intercellular adhesion molecule-3-grabbing nonintegrin; CES, carboxylesterase; IC₅₀, half maximal inhibitory concentration; iv, intravenous; D, distribution coefficient; GPE, guinea pig erythrocytes; LC-MS, liquid chromatography–mass spectrometry; MBP, mannose-binding protein; PAMPA, parallel artificial membrane permeation assay; P_{app} , apparent permeability; P_e , effective permeation; po, peroral; PPB, plasma protein binding; PSA, polar surface area; *S*, solubility; SAR, structure–activity relationship; sGF, simulated gastric fluid; sIF, simulated intestinal fluid; TEER, transepithelial resistance; UPEC, uropathogenic *E. coli*; UTI, urinary tract infection.

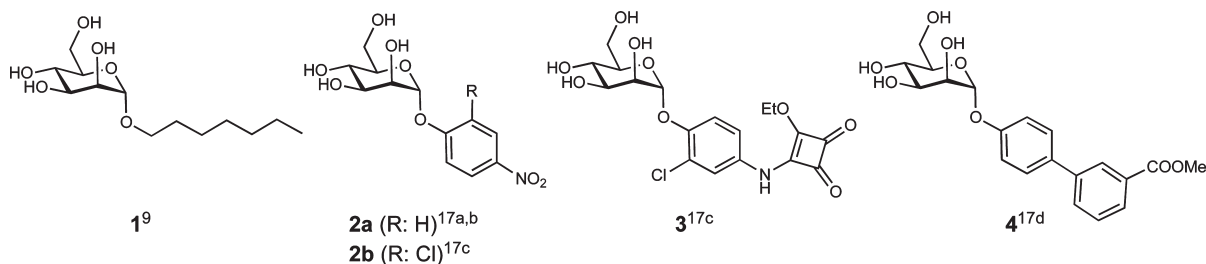
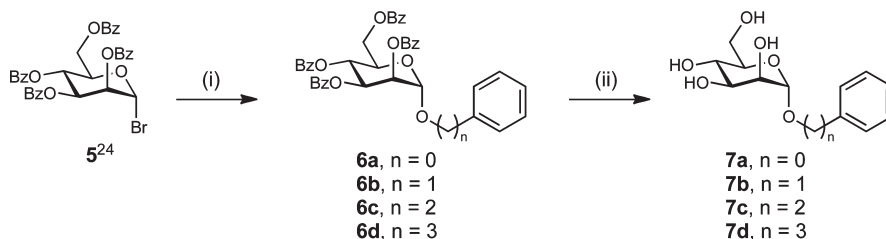


Figure 1. Known alkyl (**1**) and aryl (**2–4**) α -D-mannosides exhibiting nanomolar affinities.

Scheme 1. Phenyl α -D-Mannosides **7a–7d** with Spacers of Different Lengths between the Carbohydrate Moiety and the Phenyl Substituent^a



^a (i) $\text{Ph}(\text{CH}_2)_n\text{OH}$, $\text{Hg}(\text{CN})_2$, HgBr_2 , DCM, 2 h to 7 d, rt, 57–99%; (ii) NaOMe, MeOH, 6–16 h, rt, 48–91%.

potential antagonists for type 1 fimbriae-mediated bacterial adhesion.¹⁵ However, for these mannosides, only weak interactions in the milli- to micromolar range were observed. In contrast, numerous reports on glycoconjugate dendrimers with nanomolar affinities have been published.¹⁶ However, on the basis of their large molecular weight and high polarity, they are predicted to exhibit only poor intestinal absorption and are therefore not amenable for oral dosing. Recently, some isolated reports on high affinity monovalent FimH antagonists were published¹⁷ and, in one case, a systematic structure–activity relationship (SAR) profile was established.^{17d} In summary,^{8,9,15–19} long chain alkyl and aryl mannosides (selected examples are presented in Figure 1) displayed the highest affinity, likely due to hydrophobic interactions with two tyrosines and one isoleucine forming the entrance to the binding site, the so-called “tyrosine gate”.¹⁸ Because binding affinities were obtained from diverse assay formats,^{9,17c,20} a direct comparison of the affinities is difficult. On the basis of various crystal structures of methyl-⁸ and *n*-butyl α -D-mannoside¹⁸ as well as oligomannose-3⁹ bound to FimH, Han et al. recently presented a rationale for the design of arylmannosides with increased affinities.^{17d}

To date, a few reports on the in vivo potential of methyl α -D-mannoside^{10,21,22} and *n*-heptyl α -D-mannoside (**1**)¹⁰ are available. In all cases, the FimH antagonists were directly instilled into the bladder concomitantly with uropathogenic *E. coli* (UPEC). In this communication, we present for the first time nanomolar FimH antagonists exhibiting appropriate pharmacokinetic properties for iv and oral treatment of urinary tract infections.

Results and Discussion

Identification of Lead Mannoside. In most of the reported FimH antagonists, aromatic aglycones have been applied.¹⁷ However, only limited information on the optimal spacer length between the mannose moiety and the aromatic substituent is available. Generally, the aromatic moiety is directly fused to the anomeric oxygen.^{17a–d} Extended spacers containing one^{17b,d} or two^{17c} methylene moieties were also reported,

however, the corresponding antagonists are not really comparable to each other because different assay formats were used for their evaluation. For the identification of the optimal spacer length, we therefore synthesized mannosides **7a–d** (Scheme 1). In a competitive binding assay,²³ mannoside **7a** showed a slightly higher affinity (Table 1, entry 2) compared with **7b–7d** (see Table 1, entries 3–5), confirming recent data for **7a** and **7b**.^{17d}

From the crystal structure of *n*-butyl α -D-mannoside bound to FimH,¹⁸ it becomes obvious that the hydrophobic rim formed by Tyr48, Tyr137, and Ile52 is not reached by an anomeric phenyl group. An extension by a second aromatic ring, i.e. a biphenyl α -D-mannoside, however, should be compatible for π - π stacking. Indeed, some recently published representatives of this compound class show excellent affinities.^{17d}

To achieve an optimal fit with the hydrophobic binding site of FimH, the conformation of the biphenyl aglycone in **1** was modified by different substitution patterns on ring A (Figure 2). Because electron poor aromatic rings substantially improve the binding affinities of FimH antagonists (a 10-fold improvement is reported for **2B** vs **2A**^{17c}), chloro substituents on ring A were used for the spatial exploration of the binding site. With substituents in the *ortho*-position, only a minor change of the dihedral angle Φ_1 is observed (-3.3° to -0.7°). However, by an increased rotational barrier, the conformational flexibility is limited. The dihedral angle Φ_2 between the conjugated aromatic rings results from an interplay between π -conjugation and steric effects.^{24,25} By migrating the substituent to the *meta*-position, the torsion angle Φ_2 is substantially influenced. Whereas unsubstituted biphenyls show a global twisted minimum at a torsion angle Φ_2 of approximately 39° ,²⁶ substituents in the *meta*-position favor an increase of Φ_2 to 60° . Details of the conformational analyses are summarized in the Supporting Information.

Design Strategy for Intestinal Absorption and Renal Elimination. Besides high affinity, drug-like pharmacokinetic properties are a prerequisite for a successful in vivo application. In the present case, orally available FimH antagonists

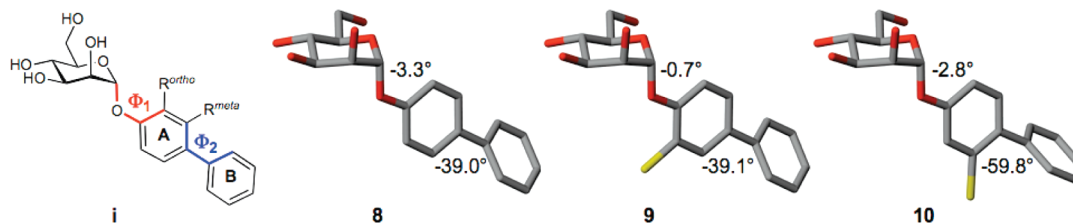


Figure 2. Conformational changes of the biphenyl aglycone by chloro substitutions in *ortho*- and *meta*-position of ring A.

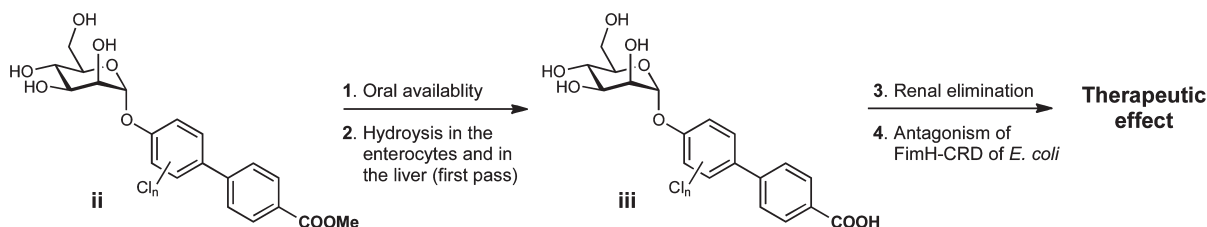


Figure 3. FimH antagonists with the pharmacodynamic and pharmacokinetic properties required for a therapeutic application. (1) For the prediction of oral availability, the PAMPA³⁰ and the Caco-2 cell assay³¹ are applied. (2) The hydrolysis of ester **ii** to carboxylate **iii** is evaluated by mouse liver microsomes. (3) Renal excretion is estimated based on a positive correlation with polar descriptors (polar surface area, H-bond donors, H-bond acceptors, rotatable bonds).³² (4) The potential of FimH antagonists is assessed with a target-based assay²³ and a function-based cellular assay.³³ For the evaluation of the therapeutic effect, a urinary tract infection mouse model (UTI mouse model in C3H/HeN mice) is applied.

that, once in circulation, are metabolically stable and undergo fast renal elimination, are required. This pharmacokinetic profile results from various serial and/or simultaneous processes that include dissolution, intestinal absorption, plasma protein binding, metabolic clearance, body distribution as well as renal and other clearance mechanisms. Because intestinal absorption and renal elimination are related to opposed properties, i.e. lipophilicity for intestinal absorption and hydrophilicity for renal elimination, a prodrug approach²⁷ was envisaged (Figure 3). Ester **ii** is expected to undergo intestinal absorption²⁸ and, later on, efficient hydrolysis to carboxylate **iii** by esterases²⁹ present in enterocytes lining the small intestine and in the liver.

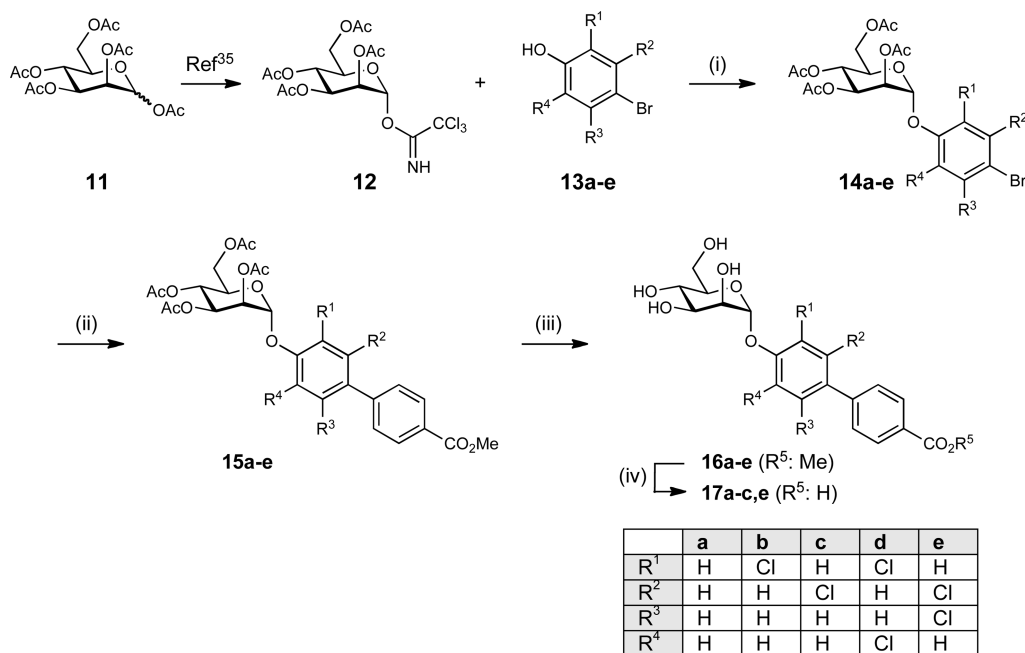
For renal clearance, the net result of glomerular filtration, active tubular secretion, and reabsorption, carboxylate **iii** should exhibit low lipophilicity ($\log D_{7.4}$) and favorable polar descriptor values (polar surface area (PSA), H-bond capacity and rotatable bonds).³² By contrast, lipophilic compounds are efficiently reabsorbed (as the passive reabsorption process occurs throughout the length of the nephron, whereas the secretion predominantly occurs at the proximal tubule). The estimated negative $\log D_{7.4}$ for antagonists of type **iii** is expected to fulfill these specifications for an efficient renal elimination and a low reabsorption. Finally, once arrived at the site of action in the bladder, the antagonist binds to the carbohydrate recognition domain (CRD) located on the bacterial pili, thus interfering with the adhesion of *E. coli* to oligosaccharide structures on urothelial cells.³⁴ To identify antagonists with the pharmacokinetic properties required for oral absorption and fast renal elimination, it was planned to determine PK parameters such as $\log D_{7.4}$, pK_a , solubility, plasma protein binding, metabolic stability, and oral availability using the parallel artificial membrane permeation assay (PAMPA)³⁰ and the Caco-2 cell assay.³¹

Synthesis of FimH Antagonists. The aglycone in the α -1-position of D-mannose plays a ternary role, i.e. it mediates the lipophilic contact with the hydrophobic tyrosine gate, contains the elements required for intestinal absorption and, after metabolic cleavage of the prodrug, for a fast renal elimination.

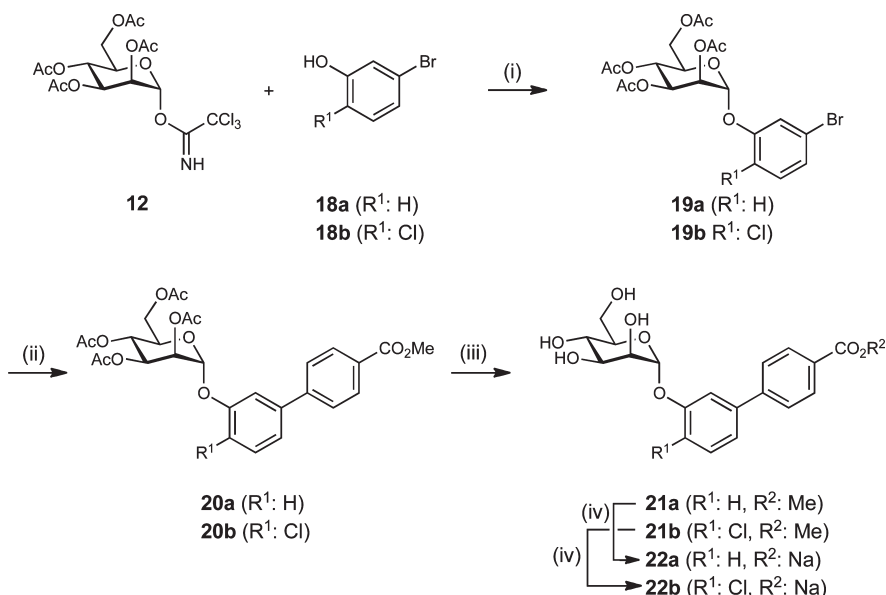
The syntheses of the *para*-substituted biphenyls **16a–e** and **17a–c,e** are outlined in Scheme 2. Lewis acid promoted glycosylation of the halogenated phenols **13a–e** with trichloroacetimidate **12**³⁵ yielded the phenyl α -D-mannosides **14a–e**. In a palladium-catalyzed Suzuki coupling with 4-methoxycarbonylphenylboronic acid, the biphenyls **15a–e** were obtained. For the deprotection of the mannose moiety, Zemplén conditions were applied (\rightarrow **16a–e**). Finally, the methyl esters were saponified, yielding the sodium salts **17a–c,e**.

In a similar approach, two *meta*-substituted biphenyls in their ester form (\rightarrow **21a,b**) and as free acids (\rightarrow **22a,b**) were obtained (see Scheme 3).

Binding Affinities and Activities. For the biological in vitro evaluation of the FimH antagonists, two assay formats have been developed. For an initial characterization, a cell-free competitive binding assay²³ and, later on, a cell-based aggregation assay,³³ were applied. Whereas in the cell-free competitive binding assay only the CRD of the pili was used, the complete pili are present in the cell-based assay format. Furthermore, both formats are competitive assays, i.e. the analyzed antagonists compete with mannosides for the binding site. In the cell-free competitive binding assay, the competitors are polymer-bound trimannosides, whereas in the aggregation assay, the antagonist competes with more potent oligo- and polysaccharide chains present on the surface of erythrocytes.³⁶ Therefore, lower IC_{50} values are expected for the cell-free competitive binding assay. In addition, switching from the cell-free target-based assay to the function-based assay generally leads to a reduction of potency by several orders of magnitude. The interaction is further complicated by the existence of a high- and a low-affinity state of the CRD of FimH. Aprikian et al. experimentally demonstrated that in full-length fimbriae the pilin domain stabilizes the CRD domain in the low-affinity state, whereas the CRD domain alone adopts the high-affinity state.³⁷ It was recently shown that the pilin domain allosterically causes a twist in the β -sandwich fold of the CRD domain, resulting in a loosening of the binding pocket.³⁸ On

Scheme 2^a

^a (i) TMSOTf, toluene, rt, 5 h (42–77%); (ii) 4-methoxycarbonylphenylboronic acid, Cs₂CO₃, Pd(PPh₃)₄, dioxane, 120°C, 8 h (28–85%); (iii) NaOMe, MeOH, rt, 4–24 h (22–86%); (iv) NaOMe, MeOH, rt, then NaOH/H₂O, rt, 16–24 h (63–94%).

Scheme 3^a

^a (i) TMSOTf, toluene, rt, 5 h (67–70%); (ii) 4-methoxycarbonylphenylboronic acid, Cs₂CO₃, Pd(PPh₃)₄, dioxane, 120°C, 8 h or Pd₂(dba)₃, S-Phos, dioxane, 80°C, overnight (46–56%); (iii) NaOMe, MeOH, rt, 24 h (52–67%); (iv) NaOMe, MeOH, rt, then NaOH/H₂O, rt, 24 h (75–95%).

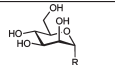
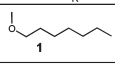
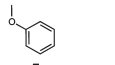
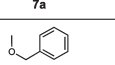
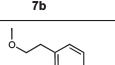
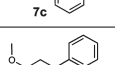
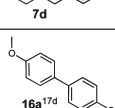
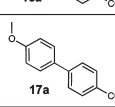
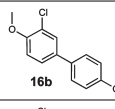
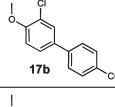
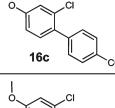
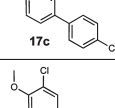
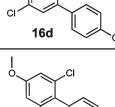
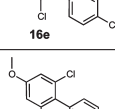
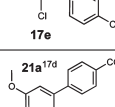
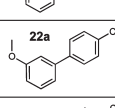
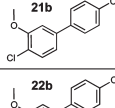
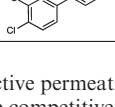
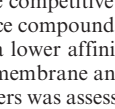
the basis of these findings, we expect a loss of affinity of our antagonists toward full-length fimbriae, when compared to the CRD domain alone.

Cell-Free Competitive Binding Assay. The cell-free inhibition assay is based on the interaction of a biotinylated polyacrylamide glycopolymer with the FimH-CRD as previously reported.²³ A recombinant protein consisting of the carbohydrate recognition domain of FimH linked with a thrombin cleavage site to a 6His-tag (FimH-CRD-Th-6His) was expressed in *E. coli* strain HM125 and purified by affinity chromatography. The IC₅₀ values of the test compounds were determined in microtiter plates coated with

FimH-CRD-Th-6His. Complexation of the biotinylated glycopolymer with streptavidin coupled to horseradish peroxidase allowed the quantification of the binding properties of FimH antagonists (Figure 4a). To ensure comparability with different antagonists, the reference compound *n*-heptyl α -D-mannopyranoside (**1**)³³ was tested in parallel in each individual microtiter plate. The affinities are reported relative to *n*-heptyl α -D-mannopyranoside (**1**) as rIC₅₀ in Table 1.

The most active representatives from the ester group are **16a** (Table 1, entry 6) and **16b** (entry 8) with affinities in the low nanomolar range, which is an approximately 10-fold improvement compared to reference compound **1**. The

Table 1. Pharmacodynamic and Pharmacokinetic Parameters of FimH Antagonists^{a,b}

		IC ₅₀ binding assay [nM]	rIC ₅₀	IC ₅₀ Aggregometry assay [μM]	PAMPA log P _e [log10 ⁶ cm/s/ %Mm]	Caco-2 P _{app} [10 ⁻⁶ cm/s]	log D _{7.4}	pK _a	log S [μg/mL]/ pH	PPB [%]
1		73±7.9	1.0	77.14±8.7	-4.89/21	nd	1.65	-	>3000	81
2		150±11.5	1.9	nd	nd/nd	nd	nd	-	>3000	nd
3		364±16.8	4.6	nd	nd/nd	nd	nd	-	nd	nd
4		210±11.2	2.6	nd	nd/nd	nd	nd	-	nd	nd
5		253±13.4	3.2	nd	nd/nd	nd	nd	-	nd	nd
6		10.4±1.2	0.14	42±7	-4.7/<20%	4.23	2.14	-	33.8/6.51	93
7		17.1±2.2	0.15	45±8	np	nd	<-1.5	3.88	>3000/6.61	73
8		4.8±1.2	0.06	9±2.7	-4.6/41.00	2.05	2.32	-	11.9/6.53	94
9		6.7±2.1	0.09	10±2.3	np/3.5	nd	-0.77	3.98	>3000/6.50	89
10		22.0±8.4	0.30	41 ¹⁾	-4.72/67.6	nd	2.42	-	11.5/6.50	95
11		27.6±3.9	0.38	17 ¹⁾	np	nd	-1.33	3.95	>3000/6.50	83
12		16.0±0.8	0.22	14 ¹⁾	-4.29/54.3	3.32	2.31	-	4.6/6.53	98
13		15.3±0.4	0.07	nd	-4.40/70.2	5.81	3.10	-	22.7/6.53	94
14		23.9±2.2	0.19	nd	nd/nd	nd	nd	nd	nd	nd
15		20.0±4.3	0.27	33 ¹⁾	-5.01/60.7	4.88	2.02	-	37.6/6.52	92
16		38.7±5.2	0.53	45 ¹⁾	np/9.7	nd	<-1.5	3.60	>3000/6.50	81
17		11.8±0.1	0.16	31 ¹⁾	-4.69/51.7	1.63	1.70	-	24.3/6.54	96
18		29.2±0.7	0.40	nd	np/nr	0.55	<-1.5	3.41	>3000/6.5	87

^a Single determination; P_e, effective permeation; P_{app}, apparent permeability; np, no permeation; nr, no retention; nd, not determined. ^b The IC₅₀s were determined with the cell-free competitive binding assay.²³ The rIC₅₀ of each substance was calculated by dividing the IC₅₀ of the compound of interest by the IC₅₀ of the reference compound **1** (entry 1). This leads to rIC₅₀ values below 1.00 for derivatives binding better than **1** and rIC₅₀ values above 1.00 for compounds with a lower affinity than **1**. The aggregation of *E. coli* and GPE were determined in the aggregometry assay.³³ Passive permeation through an artificial membrane and retention therein was determined by PAMPA (parallel artificial membrane permeation assay).³⁰ The permeation through cell monolayers was assessed by a Caco-2 assay.³¹ Distribution coefficients (log D values) were measured by a miniaturized shake flask procedure.⁴⁴ pK_a values were determined by NMR spectroscopy.⁴⁵ Plasma protein binding (PPB) was assessed by a miniaturized equilibrium dialysis protocol.⁴⁶ Thermodynamic solubility (S) was measured by an equilibrium shake flask approach.⁴⁷

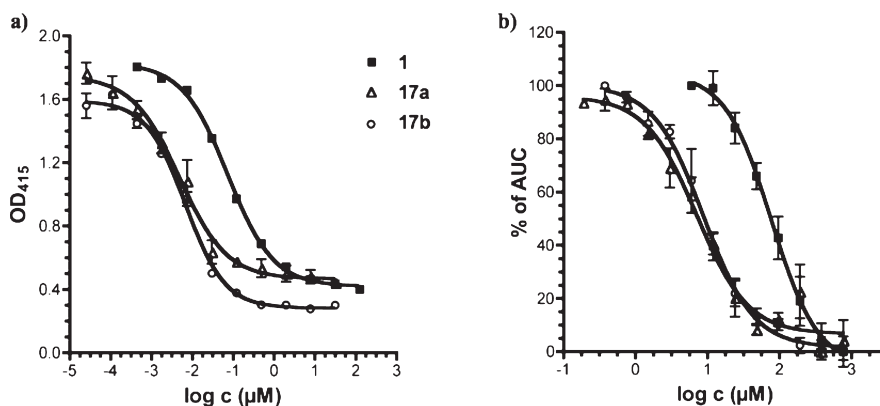


Figure 4. Affinities were determined in two different competitive assay formats. (a) a cell-free competitive binding assay²³ and (b) a cell-based aggregometry assay.³³ For antagonists **17a**, **17b**, and the reference compound **1**, IC₅₀ values in the nM and μM range, respectively, were obtained. The 1000-fold difference between the two assay formats is due to the different competitors used as well as the different affinity states present in FimH, i.e. the high-affinity state present in the CRD used in the cell-free competitive binding assay and the low-affinity state present in the pili of *E. coli* used in the aggregometry assay.

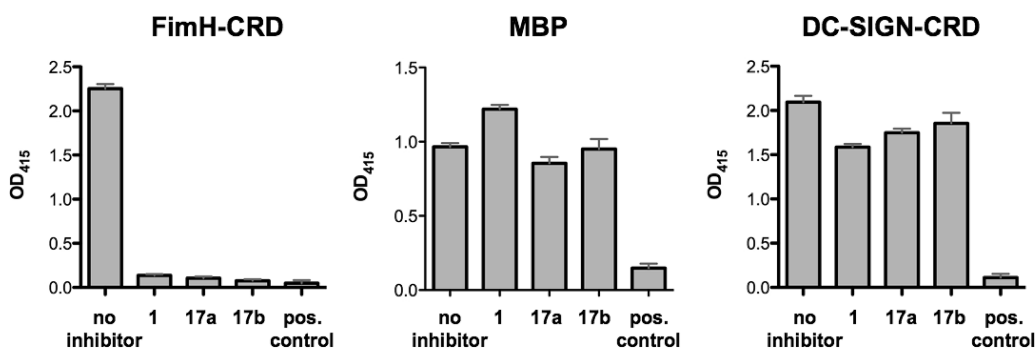


Figure 5. Competitive binding assay using FimH-CRD-Th-6His, DC-SIGN-CRD-IgG-Fc,⁴³ and MBP to evaluate the selectivity of compounds **1**, **17a**, and **17b**. Inhibitory capacities of the compounds were tested at a concentration of 1 mM. As positive control, D-mannose at a concentration of 50 mM was used.

corresponding carboxylic acids **17a** (entry 7) and **17b** (entry 9) exhibited a small reduction in affinity but are still 5-fold more active than reference compound **1**. All the remaining antagonists listed in Table 1 are slightly less active. For the in vivo examination, antagonists **17a** and **17b** were therefore foreseen for iv application and the prodrug **16b** for oral application.

Target selectivity is a further important issue. Mammalian mannose receptors are part of various biological processes, e.g. in cell–cell adhesion (DC-SIGN, dendritic cell-specific intercellular adhesion molecule-3-grabbing nonintegrin),³⁹ in the regulation of serum glycoprotein homeostasis (mannose receptor)⁴⁰ or in the innate and adaptive immune system by recognizing molecular patterns on pathogens (e.g., mannose-binding protein, mannose receptor, DC-SIGN).^{39,41,42} Non-specific interactions to the various mannose receptors by FimH inhibitors would have a profound impact on these processes. We therefore determined the affinity of reference compound **1** and the two antagonists **17a** and **17b** for two additional mannose binding proteins, DC-SIGN,^{39,43} and MBP (mannose-binding protein)⁴² (Figure 5). In both cases, affinities above 1 mM, i.e. a decrease of more than 5 orders of magnitude, was detected.

Aggregometry Assay. The potential of the biphenyl mannosides to disaggregate *E. coli* from guinea pig erythrocytes (GPE) was determined by a function-based aggregometry assay.³³ Antagonists were measured in triplicates, and the corresponding IC₅₀ values were calculated by plotting the

area under the curve (AUC) of disaggregation against the concentration of the antagonists. *n*-Heptyl α-D-mannopyranoside (**1**) was used again as reference compound and exhibits an IC₅₀ of 77.14 ± 8.7 μM. Antagonists **17a** and **17b** showed IC₅₀ values of 45 ± 8 μM and 10 ± 2.3 μM, respectively (Figure 4b). In general, the activities obtained from the aggregometry assay are approximately 1000-fold lower than the affinities determined in the target-based competitive assay (discussion see above).

In Vitro Pharmacokinetic Characterization of FimH Antagonists. For an application in the UTI mouse model, iv or po available FimH antagonists are required that, once absorbed to circulation, are metabolically stable and undergo fast renal elimination. Sufficient bioavailability requires a combination of high solubility and permeability to maximize absorption and low hepatic clearance to minimize first pass extraction. Furthermore, for efficient renal elimination, active and/or passive membrane permeability and low reabsorption in the renal tubuli is required. From the series of FimH antagonists with nanomolar in vitro activities (see Table 1), representatives with appropriate pharmacokinetic properties were selected for in vivo experiments based on the parameters shown below.

Oral Absorption and Renal Excretion. For the evaluation of oral absorption and renal excretion of the esters **16** and **21** as well as the acids **17** and **22** physicochemical parameters such as pK_a values, lipophilicity (distribution coefficients, log *D*_{7.4}), solubility, and permeability were determined

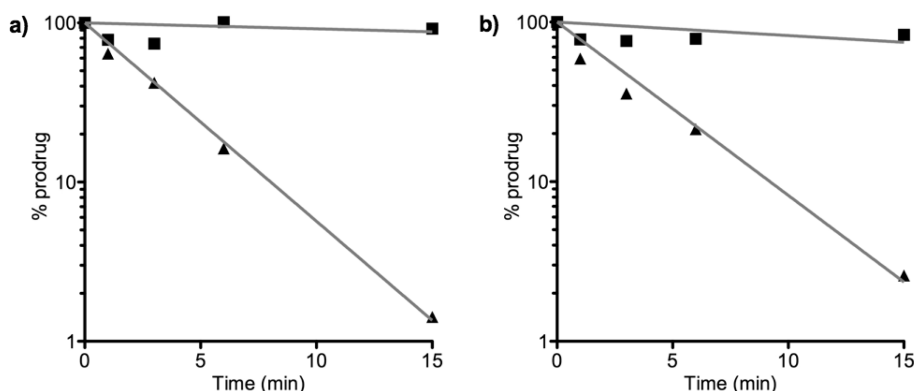


Figure 6. Incubation of (a) **16a** and (b) **16b** with pooled mouse liver microsomes (0.25 mg of protein/mL), in absence (▲) and in presence (■) of the specific carboxylesterase inhibitor bis(4-nitrophenyl) phosphate (BNPP).

(Table 1). Not surprisingly, the acids **17** and **22** showed $\log D_{7.4}$ values in the range of -1 to -2 and pK_a values of approximately 4. While these parameters are beneficial for renal excretion,³² oral absorption by passive diffusion seems unlikely. Indeed, when the permeation through an artificial membrane (PAMPA³⁰) was studied, neither significant permeation ($\log P_e$, P_e : effective permeation) nor membrane retention could be detected. Whereas for a successful oral absorption $\log P_e$ should be above -5.7 and/or the membrane retention above 80%,⁴⁸ the corresponding values for the carboxylic acids **17** and **22** are far from being in this range (see Table 1, e.g. entries 7 and 9). However, $\log D_{7.4}$ values and PAMPA results were markedly improved for the esters **16** and **21** (Table 1, e.g. entries 6 and 8), suggesting that these FimH antagonists are orally absorbed. This assumption was fully confirmed in a cell-based permeation assay with Caco-2 cells.³¹ For renal excretion, Varma et al.³¹ correlated low lipophilicity and the presence of a charged state at physiological pH positively with enhanced elimination. On the basis of $\log D_{7.4}$ and pK_a summarized in Table 1, the carboxylates **17** and **22** fulfill these requirements. Overall, these results support the prodrug approach: (i) oral application of the esters **16** and **21** and (ii) renal elimination of the corresponding acids **17** and **22**.

Solubility. A major problem of the antagonists **16** and **21** is their insufficient solubility, ranging from 4.6 to 37.6 $\mu\text{g/mL}$. Even though the solubility issue can be addressed by appropriate formulations, further structural modifications to improve solubility are necessary. Opposite to the esters, the corresponding carboxylates **17** and **22** showed excellent solubility ($> 3 \text{ mg/mL}$). This enables their iv application in physiological solutions (PBS) in the UTI model without further needs to develop suitable formulations (see below).

Stability in Simulated Gastrointestinal Fluids. To exclude degradation in the gastrointestinal tract prior to absorption, the stability of **1**, **16b**, and **17b** in simulated gastric fluid (sGF) and simulated intestinal fluid (sIF) was determined. All three antagonists proved to be sufficiently stable with more than 80% of the initial concentrations found after two hours.

Metabolic Stability. Because the prodrug approach is only applicable when the esters **16a** and **16b** are rapidly metabolically cleaved into the corresponding acids, their propensity to enzymatic hydrolysis by carboxylesterase (CES) was studied. Mammalian CESs are localized in the endoplasmic reticulum of the liver and most other organs.²⁹ Because of the excellent affinity of the corresponding acids **17a** and

17b to FimH, we concentrated our metabolic studies on the ester prodrugs **16a** and **16b**, which were incubated with pooled male mouse liver microsomes to study the hydrolysis and the release of the metabolites. Preliminary experiments involving low substrate concentrations (2 μM) and a concentration of the microsomal protein of 0.25 mg/mL showed a fast degradation of the ester prodrugs (Figure 6). Addition of the specific CES inhibitor bis(4-nitrophenyl) phosphate (BNPP) prevented ester degradation, suggesting that the metabolic transformation can be attributed to CESs.⁴⁹

On the basis of these in vitro results, we also expect fast hydrolysis of the esters in vivo at the first liver passage. Current studies are focusing on the kinetic parameters of the enzymatic ester cleavage.

To reach the minimal therapeutic concentration in the bladder (approximately 1 $\mu\text{g/mL}$, as estimated from a cell-based infection assay⁵⁰), the FimH antagonists **17a** and **17b** should be efficiently renally eliminated and not further metabolically processed. Therefore, the metabolic fate of the free carboxylic acids **17a** and **17b** was examined. A common method to predict a compound's propensity to phase I metabolism is its incubation with liver microsomes in presence of NADPH.⁵¹ Under these conditions, in vitro incubations of the free carboxylic acids **17a** and **17b** with pooled male mouse liver microsomes (0.5 mg microsomal protein/mL) did not show significant compound depletion over a period of 30 min, suggesting a high stability against cytochrome P450 mediated metabolism in vivo. However, phase II metabolic pathways such as glucuronidation remain to be studied in details.

Plasma Protein Binding (PPB). Compared to the corresponding esters **16** and **21**, the antagonists **17** and **22** exhibit 5–20% lower plasma protein binding, typically in the range of 73–89%. This rather low PPB beneficially influences renal excretion because, in line with the free drug hypothesis,⁵² molecules bound to plasma proteins evade metabolism and excretion. However, for a concluding statement, the kinetics of PPB, i.e. association and dissociation rate constants, have to be determined because PPB alone is not necessarily predictive for distribution, metabolism, and clearance.^{53,54}

In Vivo Pharmacokinetics and Treatment Studies. The two mannose derivatives methyl α -D-mannoside and *n*-heptyl α -D-mannoside (**1**) were previously tested in the UTI mouse model.^{10,21,22} In all three studies, the FimH antagonists were first preincubated with the bacterial suspension, followed by transurethral inoculation. To efficiently reduce infection,

Antagonist	Compartment	C_{\max} ($\mu\text{g/mL}$)	AUC_{0-24} ($\mu\text{g} \times \text{h/mL}$)	PPB
1	plasma	35 ± 14.1	34.3 ± 33.3	81%
	urine	951.4 ± 249.6	2469.3 ± 636.4	
17a	plasma	34.4 ± 11.8	19.3 ± 6.2	73%
	urine	509.6 ± 427.5	139.9 ± 118.8	
17b	plasma	39.4 ± 15.7	20.8 ± 7.3	89%
	urine	588.4 ± 218.2	209.6 ± 72.3	

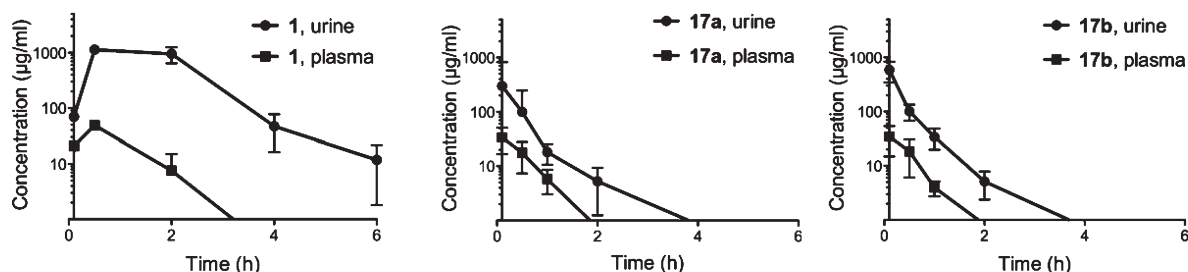


Figure 7. Determination of antagonist concentration in urine and plasma after a single iv application of 50 mg/kg. The data (table and graphs) show time-dependent urine and plasma concentrations of **1**, **17a**, and **17b**.

large amounts of methyl α -D-mannoside had to be applied (up to 1 M).²¹ For *n*-heptyl α -D-mannoside (**1**), an approximately one \log_{10} unit reduction of bacterial counts in the bladder was reached with lower, but still millimolar, concentration.¹⁰ In the previously presented studies, the FimH antagonists were exclusively instilled into the bladder, which is obviously not suitable for a therapeutic application. The aim of our project was therefore the identification of FimH antagonists suitable for iv or preferably po applications. Before infection studies in a mouse disease model could be performed, the in vivo pharmacokinetic parameters (C_{\max} , AUC) had to be determined to ensure the antagonists availability in the target organ (bladder).

Pharmacokinetics of a Single iv Application in C3H/HeN Mice. Plasma and urine concentrations of the FimH antagonists **1**, **17a**, and **17b** after iv application were determined. With a single dose of 50 mg/kg, the control compound **1** exhibited availability in the bladder over a period of 6 h after administration ($n = 4$), whereas at similar doses, **17a** and **17b** showed lower urine concentrations over a reduced time period (max 2 h) ($n = 6$). In Figure 7, the pharmacokinetic parameters are summarized. Overall, for all three compounds, higher availability of the antagonists in the urine was observed compared to the plasma. Because plasma protein binding is of comparable scale for the three compounds (see Table 1 and Figure 7), it similarly influences urine concentrations.

Pharmacokinetics of a Single po Application in C3H/HeN Mice. Aiming for an orally available FimH antagonist, the prodrug **16b** and its metabolite **17b** were tested. Because of the in vitro pharmacokinetic properties of **17b** (Table 1, entry 9), its low oral bioavailability after the administration of a single po dose (50 mg/kg) was not surprising. For the determination of the availability of a similar dose of **16b** at the target organ (bladder), plasma and urine concentrations were determined over a period of 24 h ($n = 6$) (Figure 8). Because **16b** was designed as a prodrug expected to be rapidly

Antagonist applied	Antagonist detected	Compartment	$\text{AUC}_{0-24 \text{ p.o.}}$ ($\mu\text{g} \times \text{h/mL}$)
17b	17b	Plasma	n.d.
	17b	Urine	2.7 ± 3.2
16b	16b	Plasma	1.02 ± 0.32
		Urine	1.89 ± 0.37
	17b	Plasma	2.1 ± 0.61
		Urine	21.69 ± 3.88

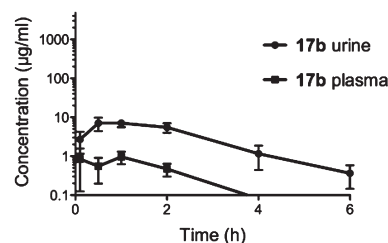


Figure 8. Determination of antagonist concentration in urine and plasma after a single po application of 50 mg/kg of antagonists **16b** and **17b**. The data (table and graph) show their time-dependent urine and plasma concentrations. When **17b** was orally applied, its plasma concentration was below the detection level, and only a small portion was present in the urine. However, after the application of the prodrug **16b**, metabolite **17b** was predominantly detected due to fast metabolic hydrolysis of **16b**. However, minor amounts of **16b** are still traceable in plasma as well as urine; nd, not detectable.

hydrolyzed, plasma and urine samples were analyzed not only for **16b** but also for its metabolite **17b**. **16b** was present only in minor concentrations in both plasma and urine. However, although the AUC of metabolite **17b** in urine is reduced by 90% compared to the iv application, its minimal therapeutic concentration can be maintained over a period of 2 to 3 h.

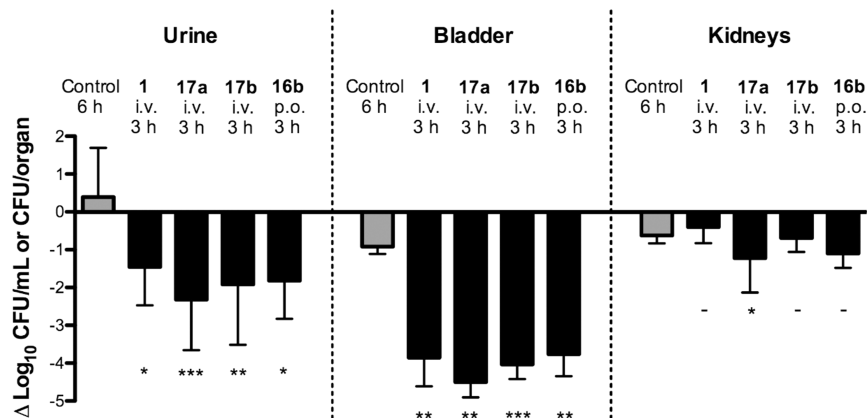


Figure 9. Treatment efficacy of the reference compound (**1**) and three FimH antagonists (**17a**, **17b**, **16b**) at a dosage of 50 mg/kg in the UTI mouse model after 3 h of infection, compared to a 6 h infection study ($n = 6$). **1**, **17a**, and **17b** were applied iv into the tail vein, whereas **16b** was applied orally. As baseline (reference), the mean counts of the 3 h infection were subtracted from the results of the tested antagonists and the 6 h control group. P values were calculated by comparing the treatment groups with the 3 h control group. (*) $P < 0.05$, (**) $P < 0.01$, (***) $P < 0.001$, (–) not significant (determined by Mann–Whitney test).

UTI Mouse Model: Treatment Study. Before treatment studies were started, the optimal infection profile was established. A 3 h infection exhibited the highest infection level in the C3H/HeN mouse strain. At longer infection times, e.g. 6 h, the control group showed indeed higher bacterial counts in the urine, however, the bladder and kidney counts already decreased due to self-clearance of the infection in the UTI mouse model.⁵⁵ For the in vivo UTI treatment studies (Figure 9), antagonists **1**, **17a**, **17b**, and **16b** were applied followed by infection with UPEC (UTI89). For each antagonist, a group of six animals was used. The animals were sacrificed 3 h after inoculation and urine and homogenized organs (bladder, kidneys) were examined for bacterial counts. The mean value in the untreated reference group ($n = 6$) showed 1.8×10^6 CFU/mL in the urine, 1.4×10^8 CFU in the bladder and 9.7×10^6 CFU in the kidneys. The bar diagram in Figure 9 summarizes the bacterial counts after iv (**1**, **17a**, and **17b**) and po (**16b**) treatment. The baseline represents the values obtained for the control group after 3 h and was used as reference for CFU reductions. **1** showed the lowest inhibition of growth in the urine with 1.5 log₁₀ CFU reduction and an approximately 4 log₁₀ reduction of bacterial counts in the bladder. After iv application of **17a**, a substantial decrease in the bacterial count was obtained (> 2 log₁₀ CFU reduction in the urine and 4.5 log₁₀ reduction in the bladder). A slightly lower reduction was observed when **17b** was applied iv (a decrease of 2 log₁₀ CFU in the urine and 4 log₁₀ for bladder counts). Interestingly, almost the same reduction of the bacterial count was detected with orally applied **16b**.

In general, urine samples showed higher bacterial counts compared to the bladder. This could be due to the difficulties during urine sampling. We observed that infected C3H/HeN mice void considerably less urine (5–50 μ L) compared to healthy mice (50–100 μ L). As a consequence, the lower urine volume leads to a higher concentration of bacteria in the collected urine and therefore to higher bacterial counts compared to the bladder.

In all treated animals, bacterial counts were only marginally reduced in the kidneys. This lower response to the treatment with FimH antagonists is probably due to different bacterial adhesion mechanisms in bladder and kidney. Whereas in the bladder adhesion is mediated by type I pili (via the CRD of FimH), P pili-dependent interactions are crucial for the adhesion in the kidneys.⁶

Summary and Conclusions

With the objective to develop an oral treatment of urinary tract infections, we have synthesized a series of potent small molecular weight FimH antagonists. Starting from the known antagonist phenyl α -D-mannopyranoside (**7a**), two equally potent classes of biphenyl α -D-mannopyranoside, those with an ester function (**16** and **21**) and those with a carboxylate (**17** and **22**) on the terminal aromatic ring, were synthesized. According to their pharmacokinetic properties, the acids **17** and **22** were not expected to be orally absorbed, a prediction that was also confirmed by an in vivo PK study. Therefore, a prodrug approach was envisaged. On the basis of permeation assays (PAMPA and Caco-2), the esters **16** and **22** were expected to exhibit oral availability. Moreover, metabolic studies with mouse liver microsomes proposed fast in vivo hydrolysis of orally applied **16b** to the corresponding carboxylate **17b**. In vivo PK studies in mice finally confirmed the in vitro prediction of a fast renal elimination of **17b** to the target organ, the bladder. When orally applied **16b** was tested in the UTI mouse model, it reduced the colony forming units (CFU) in the urine by 2 orders of magnitude and in the bladder by 4 orders of magnitude. As a result, a low molecular weight FimH antagonist suitable for the oral treatment of urinary tract infections was identified.

However, a number of parameters remain to be improved. Because the solubilities of the esters **16** and **22** are in the low μ g/mL range, an iv application was impossible and the suspension in DMSO/1% Tween 80 used for oral dosing is not optimal. In addition, due to fast renal elimination, the minimal therapeutic concentration of **17b** in the bladder could only be maintained for 2–3 h. Because high plasma protein binding was observed, an unfavorable kinetic of dissociation of the active principle from plasma proteins followed by fast renal elimination might be the reason for these findings. An improvement of the corresponding pharmacokinetic parameters should positively influence the duration of action. Furthermore, a detailed analysis of the metabolic pathway of **16b** and its metabolite **17b** will elucidate their overall metabolic fate. Finally, a detailed PK/PD profile in the mouse model will elucidate the full potential of FimH antagonists for the therapy of urinary tract infections (UTI).

Experimental Section

General Methods. NMR spectra were recorded on a Bruker Avance DMX-500 (500 MHz) spectrometer. Assignment of ¹H

and ^{13}C NMR spectra was achieved using 2D methods (COSY, HSQC, TOCSY). Chemical shifts are expressed in ppm using residual CHCl_3 , CHD_2OD , and HDO as references. Optical rotations were measured using Perkin-Elmer polarimeter 341. Electron spray ionization mass spectra (ESI-MS) were obtained on a Waters micromass ZQ. HRMS analysis were carried out using a Bruker Daltonics micrOTOF spectrometer equipped with a TOF hexapole detector. Microanalyses were performed at the Department of Chemistry, University of Basel, Switzerland. Microwave-assisted reactions were carried out with a CEM Discover and Explorer. Reactions were monitored by TLC using glass plates coated with silica gel 60 F₂₅₄ (Merck) and visualized by using UV light and/or by heating to 140 °C for 5 min with a molybdate solution (a 0.02 M solution of ammonium cerium sulfate dihydrate and ammonium molybdate tetrahydrate in aqueous 10% H_2SO_4). Column chromatography was performed on a CombiFlash Companion (Teledyne-ISCO, Inc.) using RediSep normal phase disposable flash columns (silica gel). Reversed phase chromatography was performed on LiChroprepRP-18 (Merck, 40–63 μm). Commercially available reagents were purchased from Fluka, Aldrich, Merck, AKSci, ASDI, or Alfa Aesar. Methanol (MeOH) was dried by refluxing with sodium methoxide and distilled immediately before use. Toluene was dried by filtration over Al_2O_3 (Fluka, type 5016 A basic). Dioxane was dried by distillation from sodium/benzophenone.

4-Bromophenyl 2,3,4,6-Tetra-O-acetyl- α -D-mannopyranoside (14a). To a stirred solution of **12** (1.17 g, 3.00 mmol) and 4-bromophenol (**13a**, 623 mg, 3.60 mmol) in toluene (12 mL), TMSOTf (65 μL , 0.36 mmol) was added dropwise under argon. The mixture was stirred at rt for 5 h and then diluted with toluene (15 mL) and washed with satd aq NaHCO_3 . The organic layer was separated, and the aqueous layer was extracted three times with toluene. The combined organic layers were dried over Na_2SO_4 and concentrated in vacuo. The residue was purified by flash chromatography on silica (petroleum ether/EtOAc, 19:1 to 1.5:1) to yield **14a** (1.17 g, 74%) as a white solid.

$[\alpha]_{\text{D}}^{20}$ +80.8 (*c* 1.00, CHCl_3). ^1H NMR (500 MHz, CDCl_3): δ 2.06 (s, 9H, 3 COCH₃), 2.19 (s, 3H, COCH₃), 4.06 (m, 2H, H-5, H-6a), 4.27 (dd, *J* = 5.6, 12.4 Hz, 1H, H-6b), 5.36 (t, *J* = 10.2 Hz, 1H, H-4), 5.43 (dd, *J* = 1.8, 3.5 Hz, 1H, H-2), 5.48 (d, *J* = 1.7 Hz, 1H, H-1), 5.53 (dd, *J* = 3.5, 10.1 Hz, 1H, H-3), 6.98, 7.41 (AA', BB' of AA'BB', *J* = 9.0 Hz, 4H, C₆H₄). ^{13}C NMR (125 MHz, CDCl_3): δ 20.71, 20.73, 20.74, 20.9 (4 COCH₃), 62.1 (C-6), 65.9 (C-4), 68.8 (C-3), 69.2 (C-2), 69.3 (C-5), 95.9 (C-1), 115.6, 118.3, 132.6, 154.7 (6C, C₆H₄), 170.0 (4C, 4 CO).

4-Bromo-2-chlorophenyl 2,3,4,6-tetra-O-acetyl- α -D-mannopyranoside (14b). According to the procedure described for **14a**, compound **12** (2.38 g, 4.84 mmol) and 4-bromo-2-chlorophenol (**13b**, 1.20 g, 5.80 mmol) were treated with TMSOTf (107 mg, 0.484 mmol) to yield **14b** (1.54 g, 59%) as a white solid.

$[\alpha]_{\text{D}}^{20}$ +60.6 (*c* 0.40, CHCl_3). ^1H NMR (500 MHz, CDCl_3): δ 2.02, 2.04, 2.18 (3s, 12H, 4 COCH₃), 4.05 (dd, *J* = 2.3, 12.2 Hz, 1H, H-6a), 4.10 (ddd, *J* = 2.7, 5.3, 9.6 Hz, 1H, H-5), 4.24 (dd, *J* = 5.4, 12.2 Hz, 1H, H-6b), 5.35 (t, *J* = 10.1 Hz, 1H, H-4), 5.48 (m, 2H, H-1, H-2), 5.56 (dd, *J* = 3.2, 10.1 Hz, 1H, H-3), 7.03 (d, *J* = 8.8 Hz, 1H, C₆H₃), 7.30 (dd, *J* = 2.4, 8.8 Hz, 1H, C₆H₃), 7.53 (d, *J* = 2.4 Hz, 1H, C₆H₃). ^{13}C NMR (125 MHz, CDCl_3): δ 20.9, 21.1 (4C, 4 COCH₃), 62.3 (C-6), 65.9 (C-4), 68.9 (C-3), 69.4 (C-2), 70.1 (C-5), 96.9 (C-1), 115.9, 118.4, 125.7, 130.8, 133.3, 150.6 (C₆H₃), 169.9, 170.0, 170.1, 170.7 (4 CO). ESI-MS calcd for $\text{C}_{20}\text{H}_{22}\text{BrClNaO}_{10}$ [*M* + *Na*]⁺ 559.0; found 559.0; Anal. Calcd for $\text{C}_{20}\text{H}_{22}\text{BrClO}_{10}$: C 44.67, H 4.12. Found: C 45.08, H 4.14.

Methyl 4'-(2,3,4,6-Tetra-O-acetyl- α -D-mannopyranosyloxy)-biphenyl-4-carboxylate (15a). A Schlenk tube was charged with **14a** (503 mg, 1.00 mmol), 4-methoxycarbonylphenylboronic acid (224 mg, 1.24 mmol), S-Phos (20.5 mg, 0.05 mmol), cesium carbonate (1.17 g, 3.6 mmol), Pd₂(dba)₃ (10.4 mg, 0.01 mmol), and a stirring bar. The tube was closed with a rubber septum and was evacuated and flushed with argon. This procedure was

repeated once, and then freshly degassed dioxane (5 mL) was added under a stream of argon. The reaction tube was quickly sealed and the contents were stirred at 80 °C overnight. The reaction mixture was cooled to rt, diluted with EtOAc (10 mL), washed with satd aq NaHCO_3 (5 mL) and brine (5 mL), and dried over Na_2SO_4 . The solvents were removed in vacuo, and the residue was purified by flash chromatography on silica (petroleum ether/EtOAc, 3:1 to 3:2) to give **15a** (474 mg, 85%) as a white solid.

$[\alpha]_{\text{D}}^{20}$ +80.8 (*c* 1.00, CHCl_3). ^1H NMR (500 MHz, CDCl_3): δ 2.02, 2.03, 2.04, 2.19 (4s, 12H, COCH₃), 3.91 (s, 3H, OCH₃), 4.08 (m, 2H, H-6a, H-5), 4.27 (dd, *J* = 5.2, 12.2 Hz, 1H, H-6b), 5.37 (t, *J* = 10.1 Hz, 1H, H-4), 5.45 (dd, *J* = 1.8, 3.4 Hz, 1H, H-2), 5.56 (m, 2H, H-1, H-3), 7.16 (AA' of AA'BB', *J* = 8.7 Hz, 2H, C₆H₄), 7.57 (m, 4H, C₆H₄), 8.07 (BB' of AA'BB', *J* = 8.4 Hz, 2H, C₆H₄). ^{13}C NMR (125 MHz, CDCl_3): δ 20.74, 20.75, 20.77, 21.0 (4 COCH₃), 52.2 (OCH₃), 62.1 (C-6), 65.9 (C-4), 68.9 (C-3), 69.3, 69.4 (C-2, C-5), 95.8 (C-1), 116.9, 126.7, 128.5, 128.7, 130.2, 134.8, 144.8, 155.7 (12C, 2 C₆H₄), 167.0, 169.8, 170.0, 170.1, 170.6 (5 CO). ESI-MS calcd for $\text{C}_{28}\text{H}_{30}\text{NaO}_{12}$ [*M* + *Na*]⁺ 581.2; found 581.0.

Methyl 4'-(2,3,4,6-Tetra-O-acetyl- α -D-mannopyranosyloxy)-3'-chlorobiphenyl-4-carboxylate (15b). A microwave tube was charged with bromide **14b** (720 mg, 1.34 mmol), 4-methoxycarbonylphenylboronic acid (289 mg, 1.61 mmol), cesium carbonate (1.31 g, 4.02 mmol), and Pd(PPh₃)₄ (77.4 mg, 0.067 mmol). The tube was sealed with a Teflon septum, evacuated through a needle, and flushed with argon. Degassed dioxane (1.5 mL) was added and the closed tube was degassed in an ultrasonic bath for 15 min, flushed again with argon for 20 min, and exposed to microwave irradiation at 120 °C for 500 min. The solvent was evaporated in vacuo. The residue was dissolved in DCM (10 mL), washed with brine (2 × 10 mL), dried over Na_2SO_4 , and concentrated in vacuo. The residue was purified by flash chromatography on silica (petroleum ether/EtOAc, 5:1 to 0.5:1) to yield **15b** (333 mg, 42%) as a white foam.

$[\alpha]_{\text{D}}^{20}$ +66.3 (*c* 1.06, CHCl_3). ^1H NMR (500 MHz, CDCl_3): δ 2.03, 2.06, 2.20 (3s, 12H, COCH₃), 3.92 (s, 3H, OCH₃), 4.08 (dd, *J* = 2.4, 12.3 Hz, 1H, H-6a), 4.17 (m, 1H, H-5), 4.28 (dd, *J* = 5.4, 12.3 Hz, 1H, H-6b), 5.39 (t, *J* = 10.6 Hz, 1H, H-4), 5.54 (dd, *J* = 1.9, 3.4 Hz, 1H, H-2), 5.59 (d, *J* = 1.8 Hz, 1H, H-1), 5.62 (dd, *J* = 3.5, 10.1 Hz, 1H, H-3), 7.24 (s, 1H, C₆H₃), 7.44 (dd, *J* = 2.2, 8.5 Hz, 1H, C₆H₃), 7.57 (AA' of AA'BB', *J* = 8.5 Hz, 2H, C₆H₄), 7.65 (d, *J* = 2.2 Hz, 1H, C₆H₃), 8.08 (BB' of AA'BB', *J* = 8.5 Hz, 2H, C₆H₄). ^{13}C NMR (125 MHz, CDCl_3): δ 20.9, 21.0, 21.1 (4C, 4 COCH₃), 52.5 (OCH₃), 62.3 (C-6), 66.0 (C-4), 69.0 (C-3), 69.5 (C-2), 70.0 (C-5), 96.8 (C-1), 117.4, 126.7, 126.9, 129.5, 130.5, 136.4, 143.6, 151.3 (12C, C₆H₃, C₆H₄), 167.0, 169.9, 170.0, 170.2, 170.7 (5 CO). ESI-MS calcd for $\text{C}_{28}\text{H}_{29}\text{ClNaO}_{12}$ [*M* + *Na*]⁺ 615.1; found 615.2. Anal. Calcd for $\text{C}_{28}\text{H}_{29}\text{ClO}_{12}$: C 56.71, H 4.93. Found: C 56.79, H 4.92.

Methyl 4'-(α -D-Mannopyranosyloxy)-biphenyl-4-carboxylate (16a). ^{17d} To a solution of **15a** (170 mg, 0.304 mmol) in MeOH (3 mL) was added freshly prepared 1 M NaOMe in MeOH (100 μL) under argon. The mixture was stirred at rt until the reaction was complete (monitored by TLC), then neutralized with Amberlyst-15 (H⁺) ion-exchange resin, filtered, and concentrated in vacuo. The residue was purified by reversed-phase chromatography (RP-18, H₂O/MeOH, 1:0–1:1) to give **16a** (90 mg, 76%) as white solid.

$[\alpha]_{\text{D}}^{20}$ +82.8 (*c* 0.2, MeOH). ^1H NMR (500 MHz, CD_3OD): δ 3.62 (m, 1H, H-5), 3.72 (m, 3H, H-4, H-6a, H-6b), 3.92 (m, 4H, H-3, OCH₃), 4.03 (s, 1H, H-2), 5.55 (s, 1H, H-1), 7.24 (AA' of AA'BB', *J* = 8.0 Hz, 2H, C₆H₄), 7.64 (AA' of AA'BB', *J* = 7.5 Hz, 2H, C₆H₄), 7.71 (BB' of AA'BB', *J* = 8.0 Hz, 2H, C₆H₄), 8.07 (BB' of AA'BB', *J* = 7.5 Hz, 2H, C₆H₄). ^{13}C NMR (125 MHz, CD_3OD): δ 52.6 (OCH₃), 62.7 (C-6), 68.3 (C-4), 72.0 (C-2), 72.4 (C-3), 75.5 (C-5), 100.1 (C-1), 118.2, 127.7, 131.1, 135.1, 146.6, 158.2, 160.3 (12C, 2 C₆H₄), 166.1 (CO). HR-MS calcd for $\text{C}_{20}\text{H}_{22}\text{NaO}_8$ [*M* + *Na*]⁺ 413.1212; found 413.1218.

Methyl 3'-Chloro-4'-(α -D-mannopyranosyloxy)-biphenyl-4-carboxylate (16b). According to the procedure described for **16a**, compound **16b** was prepared from **15b** (764 mg, 1.29 mmol). Yield: 69 mg, 12%.

$[\alpha]_D^{25} +97.4$ (c 1.01, MeOH). $^1\text{H NMR}$ (500 MHz, CD_3OD): δ 3.64 (m, 1H, H-5), 3.72 (m, 1H, H-6a), 3.78 (m, 2H, H-4, H-6b), 3.91 (s, 3H, OCH_3), 4.00 (dd, $J=3.4, 9.5$ Hz, 1H, H-3), 4.11 (dd, $J=1.8, 3.1$ Hz, 1H, H-2), 5.60 (d, $J=1.1$ Hz, 1H, H-1), 7.46 (d, $J=8.6$ Hz, 1H, C_6H_3), 7.58 (dd, $J=2.2, 8.6$ Hz, 1H, C_6H_3), 7.69 (AA' of AA'BB', $J=8.4$ Hz, 2H, C_6H_4), 7.72 (d, $J=2.2$ Hz, 1H, C_6H_3), 8.08 (BB' of AA'BB', $J=8.4$ Hz, 2H, C_6H_4). $^{13}\text{C NMR}$ (125 MHz, CD_3OD): δ 52.7 (OCH_3), 62.8 (C-6), 68.3 (C-4), 71.9 (C-2), 72.5 (C-3), 76.2 (C-5), 100.8 (C-1), 118.7, 125.58, 127.8, 127.9, 129.9, 130.3, 131.3, 136.4, 145.3, 153.5 (12C, C_6H_3 , C_6H_4), 168.4 (CO). HR-MS calcd for $\text{C}_{20}\text{H}_{21}\text{ClNaO}_8$ [$\text{M} + \text{Na}$] $^+$ 447.0823; found 447.082.

Sodium 4'-(α -D-Mannopyranosyloxy)-biphenyl-4-carboxylate (17a). To a solution of **15a** (228 mg, 0.408 mmol) in MeOH (6.0 mL) was added 1 M NaOMe in MeOH (60 μL) at rt. The reaction mixture was stirred at rt for 4 h, and then NaOH (82 mg) in water (6 mL) was added and stirring was continued at rt overnight. The reaction mixture was concentrated in vacuo, and the residue was purified by reversed-phase chromatography (RP-18, $\text{H}_2\text{O}/\text{MeOH}$, 1:0–1:1) to afford **17a** (96 mg, 63%) as a white solid.

$[\alpha]_D^{25} +103$ (c 0.10, MeOH). $^1\text{H NMR}$ (500 MHz, CD_3OD): δ 3.60 (m, 1H, H-5), 3.72 (m, 3H, H-6a, H-6b, H-4), 3.89 (dd, $J=3.4, 9.5$ Hz, 1H, H-3), 4.00 (dd, $J=1.8, 3.3$ Hz, 1H, H-2), 5.51 (s, 1H, H-1), 7.19, 7.60 (AA', BB' of AA'BB', $J=8.7$ Hz, 4H, C_6H_4), 8.01 (d, $J=8.2$ Hz, 2H, C_6H_4), 8.46 (s, 2H, C_6H_4). $^{13}\text{C NMR}$ (125 MHz, CD_3OD): δ 63.2 (C-6), 68.9 (C-4), 72.6 (C-2), 73.0 (C-3), 76.1 (C-5), 100.7 (C-1), 118.7, 128.0, 129.9, 131.8 (12C, 2 C_6H_4). HR-MS calcd for $\text{C}_{19}\text{H}_{20}\text{NaO}_8$ [$\text{M} + \text{H}$] $^+$ 399.1056; found 399.1052.

Sodium 3'-Chloro-4'-(α -D-mannopyranosyloxy)-biphenyl-4-carboxylate (17b). To a solution of **15b** (380 mg, 0.641 mmol) in MeOH (10 mL) was added 1 M NaOMe in MeOH (300 μL). After stirring at rt for 24 h, 0.5 M aq NaOH (18 mL) was added and stirring continued for another 24 h. The solution was concentrated in vacuo and the residue was purified by reversed-phase chromatography (RP-18, $\text{H}_2\text{O}/\text{MeOH}$, 1:0–1:1) to yield **17b** (222 mg, 80%) as a white solid.

$[\alpha]_D^{25} +61.6$ (c 1.00, H_2O). $^1\text{H NMR}$ (500 MHz, D_2O): δ 3.66 (m, 1H, H-5), 3.73 (m, 2H, H-6a, H-6b), 3.79 (t, $J=9.8$ Hz, 1H, H-4), 4.07 (dd, $J=3.4, 9.8$ Hz, 1H, H-3), 4.14 (d, $J=1.4$ Hz, 1H, H-2), 5.47 (bs, 1H, H-1), 7.04 (d, $J=8.6$ Hz, 1H, C_6H_3), 7.24 (d, $J=8.6$ Hz, 1H, C_6H_3), 7.37 (AA' of AA'BB', $J=8.1$ Hz, 2H, C_6H_4), 7.41 (bs, 1H, C_6H_3), 7.86 (BB' of AA'BB', $J=8.1$ Hz, 2H, C_6H_4). $^{13}\text{C NMR}$ (125 MHz, D_2O): δ 60.6 (C-6), 66.5 (C-4), 69.0 (C-2), 70.5 (C-3), 73.9 (C-5), 98.6 (C-1), 117.5, 123.9, 126.2, 126.4, 128.4, 129.6, 135.2, 135.3, 141.0, 150.4 (12C, C_6H_3 , C_6H_4), 175.0 (CO). HR-MS calcd for $\text{C}_{19}\text{H}_{18}\text{ClNaO}_8$ [$\text{M} + \text{H}$] $^+$ 433.0666; found 433.0670.

Competitive Binding Assay. A recombinant protein consisting of the CRD of FimH linked with a thrombin cleavage site to a 6His-tag (FimH-CRD-Th-6His) was expressed in *E. coli* strain HM125 and purified by affinity chromatography.²³ To determine the affinity of the various FimH antagonists, a competitive binding assay described previously²³ was applied. Microtiter plates (F96 MaxiSorp, Nunc) were coated with 100 $\mu\text{L}/\text{well}$ of a 10 $\mu\text{g}/\text{mL}$ solution of FimH-CRD-Th-6His in 20 mM HEPES, 150 mM NaCl, and 1 mM CaCl_2 , pH 7.4 (assay buffer) overnight at 4 $^\circ\text{C}$. The coating solution was discarded and the wells were blocked with 150 $\mu\text{L}/\text{well}$ of 3% BSA in assay buffer for 2 h at 4 $^\circ\text{C}$. After three washing steps with assay buffer (150 $\mu\text{L}/\text{well}$), a 4-fold serial dilution of the test compound (50 $\mu\text{L}/\text{well}$) in assay buffer containing 5% DMSO and streptavidin-peroxidase coupled Man- α (1-3)-[Man- α (1-6)]-Man- β (1-4)-GlcNAc- β (1-4)-GlcNAc β polyacrylamide (TM-PAA) polymer (50 $\mu\text{L}/\text{well}$ of a 0.5 $\mu\text{g}/\text{mL}$ solution) were added. On each individual microtiter plate, *n*-heptyl α -D-mannopyranoside (**1**) was tested in parallel.

The plates were incubated for 3 h at 25 $^\circ\text{C}$ and 350 rpm and then carefully washed four times with 150 $\mu\text{L}/\text{well}$ assay buffer. After the addition of 100 $\mu\text{L}/\text{well}$ of 2,2'-azino-di-(3-ethylbenzthiazoline-6-sulfonic acid) (ABTS)-substrate, the colorimetric reaction was allowed to develop for 4 min and then stopped by the addition of 2% aqueous oxalic acid before the optical density (OD) was measured at 415 nm on a microplate-reader (Spectramax 190, Molecular Devices, California, USA). The IC_{50} values of the compounds tested in duplicates were calculated with prism software (GraphPad Software, Inc., La Jolla, California, USA). The IC_{50} defines the molar concentration of the test compound that reduces the maximal specific binding of TM-PAA polymer to FimH-CRD by 50%. The relative IC_{50} (rIC_{50}) is the ratio of the IC_{50} of the test compound to the IC_{50} of *n*-heptyl α -D-mannopyranoside (**1**).

Selectivity for FimH vs Mannose-Binding Protein and DC-SIGN. Recombinant FimH-CRD-Th-6His (10 $\mu\text{g}/\text{mL}$), DC-SIGN-CRD-Fc-IgG³⁹ (2.5 $\mu\text{g}/\text{mL}$), and mannose-binding protein⁴² (MBP, 10 $\mu\text{g}/\text{mL}$, R&D Systems, Minneapolis, MN) were each diluted in assay buffer (20 mM HEPES, pH 7.4, 150 mM NaCl, and 10 mM CaCl_2) and were coated on microtiter plates (F96 MaxiSorp, Nunc) with 100 $\mu\text{L}/\text{well}$ overnight at 4 $^\circ\text{C}$. The further steps were performed as described above.

Aggregometry Assay. The aggregometry assay was carried out as previously described.³³ In short, the percentage of aggregation of *E. coli* UTI89 with guinea pig erythrocytes (GPE) was quantitatively determined by measuring the optical density at 740 nm and 37 $^\circ\text{C}$ under stirring at 1000 rpm using an APACT 4004 aggregometer (Endotell AG, Allschwil, Switzerland). Bacteria were cultivated as described below (see in vivo models). GPE were separated from guinea pig blood (Charles River Laboratories, Sulzfeld, Germany) using Histopaque (density of 1.077 g/mL at 24 $^\circ\text{C}$, Sigma-Aldrich, Buchs, Switzerland). Prior to the measurements, the cell densities of *E. coli* and GPE were adjusted to an OD_{600} of 4, corresponding to 1.9×10^8 CFU/mL and 2.2×10^6 cells/mL, respectively. For the calibration of the instrument, the aggregation of protein-poor plasma (PPP) using PBS alone was set as 100% and the aggregation of protein-rich plasma (PRP) using GPE as 0%. After calibration, measurements were performed with 250 μL of GPE and 50 μL of bacterial suspension and the aggregation monitored over 600 s. After the aggregation phase of 600 s, 25 μL of antagonist in PBS was added to each cuvette and disaggregation was monitored for 1400 s. UTI89 $\Delta\text{fimA-H}$ was used as negative control.

Determination of the Pharmacokinetic Parameters. Materials. Dimethyl sulfoxide (DMSO), 1-octanol, pepsin, pancreatin, reduced nicotinamide adenine dinucleotide phosphate (NADPH), Dulbecco's Modified Eagle's Medium (DMEM) high glucose, and bis(4-nitrophenyl) phosphate (BNPP) were purchased from Sigma-Aldrich (Sigma-Aldrich, St. Louis MO, USA). PAMPA System Solution, GIT-0 Lipid Solution, and Acceptor Sink Buffer were ordered from pIon (pIon, Woburn MA, USA). L-Glutamine-200 mM (100 \times) solution, MEM nonessential amino acid (MEM-NEAA) solution, fetal bovine serum (FBS), and DMEM without sodium pyruvate and phenol red were bought from Invitrogen (Invitrogen, Carlsbad CA, USA). Human plasma was bought from Biopredic (Biopredic, Rennes, France) and acetonitrile (MeCN) from Acros (Acros Organics, Geel, Belgium). Pooled male mouse liver microsomes were purchased from BD Bioscience (BD Bioscience, Woburn, MA, USA). Magnesium chloride was bought from Fluka (Fluka Chemie GmbH, Buchs, Switzerland). Tris(hydroxymethyl)-aminomethane (TRIS) was obtained from AppliChem (AppliChem, Darmstadt, Germany). The Caco-2 cells were kindly provided by Prof G. Imanidis, FHNW, Muttens, and originated from the American Type Culture Collection (Rockville, MD, USA).

log $D_{7.4}$ Determination. The in silico prediction tool ALOGPS 2.1⁵⁶ was used to estimate the log P values of the compounds. Depending on these values, the compounds were classified into three categories: hydrophilic compounds (log P

Table 2

compound type	log <i>P</i>	ratios (1-octanol:buffer)
hydrophilic	< 0	30:140, 40:130
moderately lipophilic	0–1	70:110, 110:70
lipophilic	> 1	3:180, 4:180

below zero), moderately lipophilic compounds (log *P* between zero and one) and lipophilic compounds (log *P* above one). For each category, two different ratios (volume of 1-octanol to volume of buffer) were defined as experimental parameters (Table 2):

Equal amounts of phosphate buffer (0.1 M, pH 7.4) and 1-octanol were mixed and shaken vigorously for 5 min to saturate the phases. The mixture was left until separation of the two phases occurred, and the buffer was retrieved. Stock solutions of the test compounds were diluted with buffer to a concentration of 1 μM. For each compound, six determinations, i.e., three determinations per 1-octanol:buffer ratio, were performed in different wells of a 96-well plate. The respective volumes of buffer containing analyte (1 μM) were pipetted to the wells and covered by saturated 1-octanol according to the chosen volume ratio. The plate was sealed with aluminum foil, shaken (1350 rpm, 25 °C, 2 h) on a Heidolph Titramax 1000 plate-shaker (Heidolph Instruments GmbH & Co. KG, Schwabach, Germany) and centrifuged (2000 rpm, 25 °C, 5 min, 5804 R Eppendorf centrifuge, Hamburg, Germany). The aqueous phase was transferred to a 96-well plate for analysis by liquid chromatography–mass spectrometry (LC-MS).

log *D*_{7.4} was calculated from the 1-octanol:buffer ratio (*o*:*b*), the initial concentration of the analyte in buffer (1 μM), and the concentration of the analyte in buffer (*c*_B) with equilibration:

$$\log D_{7.4} = \log \left(\frac{1 \mu\text{M} - c_B}{c_B} \times \frac{1}{o:b} \right)$$

The average of the three log *D*_{7.4} values per 1-octanol:buffer ratio was calculated. If the two mean values obtained for a compound did not differ by more than 0.1 unit, the results were accepted.

Parallel Artificial Membrane Permeation Assay (PAMPA). log *P*_e was determined in a 96-well format with the PAMPA³⁰ permeation assay. For each compound, measurements were performed at three pH values (5.0, 6.2, 7.4) in quadruplicates. For this purpose, 12 wells of a deep well plate, i.e., four wells per pH value, were filled with 650 μL of System Solution. Samples (150 μL) were withdrawn from each well to determine the blank spectra by UV-spectroscopy (SpectraMax 190, Molecular Devices, Silicon Valley CA, USA). Then, analyte dissolved in DMSO was added to the remaining System Solution to yield 50 μM solutions. To exclude precipitation, the optical density was measured at 650 nm, with 0.01 being the threshold value. Solutions exceeding this threshold were filtrated. Afterward, samples (150 μL) were withdrawn to determine the reference spectra. A further 200 μL were transferred to each well of the donor plate of the PAMPA sandwich (pIon, Woburn MA, USA, P/N 110 163). The filter membranes at the bottom of the acceptor plate were impregnated with 5 μL of GIT-0 Lipid Solution and 200 μL of Acceptor Sink Buffer were filled into each acceptor well. The sandwich was assembled, placed in the GutBox, and left undisturbed for 16 h. Then, it was disassembled and samples (150 μL) were transferred from each donor and acceptor well to UV-plates. Quantification was performed by both UV-spectroscopy and LC-MS. log *P*_e values were calculated with the aid of the PAMPA Explorer Software (pIon, version 3.5).

Colorectal Adenocarcinoma Cells (Caco-2 Cells) Permeation Assay. The cells were cultivated in tissue culture flasks (BD Biosciences, Franklin Lakes NJ, USA) with DMEM high glucose medium, containing 1% L-glutamine solution, 1% MEM-NEAA solution, and 10% FBS. The cells were kept at

37 °C in humidified air containing 8% CO₂, and the medium was changed every second to third day. When approximately 90% confluence was reached, the cells were split in a 1:10 ratio and distributed to new tissue culture flasks. At passage numbers between 60 and 65, they were seeded at a density of 5.33 × 10⁵ cells per well to Transwell 6-well plates (Corning Inc., Corning NY, USA) with 2.5 mL of culture medium in the basolateral compartment and 1.5 mL (days 1–10) or 1.8 mL (from day 10 on) in the basolateral compartment. The medium was renewed on alternate days. Experiments were performed between days 19 and 21 postseeding. DMEM without sodium pyruvate and phenol red was used as transport medium for experiments. Previous to the experiment, the integrity of the Caco-2 monolayers was evaluated by measuring the transepithelial resistance (TEER) in transport medium (37 °C) with an Endohm tissue resistance instrument (World Precision Instruments Inc., Sarasota, FL, USA). Only wells with TEER values higher than 300 Ωcm² were used. Experiments were performed in triplicates. Transport medium (10 μL) from the apical compartments of three wells were replaced by the same volume of compound stock solutions (10 mM). The Transwell plate was then shaken (250 rpm) in the incubator. Samples (100 μL) were withdrawn after 5, 15, 30, 60, and 120 min from the basolateral compartment and concentrations were analyzed by HPLC. Apparent permeability coefficients (*P*_{app}) were calculated according to the following equation

$$P_{\text{app}} = \frac{dQ}{dt} \times \frac{1}{A \times c_0}$$

where *dQ/dt* is the permeability rate, *A* the surface area of the monolayer, and *c*₀ the initial concentration in the donor compartment.³¹ After the experiment, TEER values were assessed again for every well and results from wells with values below 300 Ωcm² were discarded.

p*K*_a Values. The p*K*_a values were determined as described elsewhere.⁴⁵ Briefly, the pH of a sample solution was gradually changed and the chemical shift of protons adjacent to ionizable centers was monitored by ¹H nuclear magnetic resonance (NMR) spectroscopy. The shift was plotted against the pH of the respective sample, and the p*K*_a was read out from the inflection point of the resulting sigmoidal curve.

Plasma Protein Binding (PPB). The dialysis membranes (HTDialysis LCC, Gales Ferry, CT, USA; MWCO 12–14 K) were prepared according to company instructions. The human plasma was centrifuged (5800 rpm, 25 °C, 10 min), the pH of the centrifugate (without floating plasma lipids) was adjusted to 7.5, and analyte was added to yield 10 μM solutions. Equal volumes (150 μL) of phosphate buffer (0.1 M, pH 7.5) and analyte-containing plasma were transferred to the separated compartments of the assembled 96-well high throughput dialysis block (HTDialysis LCC, Gales Ferry, CT, USA). Measurements were performed in triplicates. The plate was covered with a sealing film and incubated (5 h, 37 °C). Buffer and plasma compartment were processed separately. From the buffer compartments, 90 μL were withdrawn and 10 μL of blank plasma were added. From the plasma compartments, 10 μL were withdrawn and 90 μL of blank buffer were added. After protein precipitation with 300 μL ice-cooled MeCN, the solutions were mixed, centrifuged (3600 rpm, 4 °C, 11 min), and 50 μL of the supernatant were retrieved. Analyte concentrations were determined by LC-MS. The fraction bound (*f*_b) was calculated as follows:

$$f_b = 1 - \frac{c_b}{c_p}$$

where *c*_b is the concentration in the buffer and *c*_p the concentration in the plasma compartment. Values were accepted if the recovery of analyte was between 80 and 120%.

Thermodynamic Solubility. Microanalysis tubes (Labo-Tech J. Stofer LTS AG, Muttenz, Switzerland) were charged with

1 mg of solid substance and 250 μ L of phosphate buffer (50 mM, pH 6.5). The samples were briefly shaken by hand and then sonicated for 15 min and vigorously shaken (600 rpm, 25 °C, 2 h) on a Eppendorf Thermomixer Comfort. Afterward, the samples were left undisturbed for 24 h. After measuring the pH, the saturated solutions were filtered through a filtration plate (MultiScreen HTS, Millipore, Billerica MA, USA) by centrifugation (1500 rpm, 25 °C, 3 min). Prior to concentration determination by LC-MS, the filtrates were diluted (1:1, 1:10 and 1:100 or, if the results were outside of the calibration range, 1:1000 and 1:10000). The calibration was based on six values ranging from 0.1 to 10 μ g/mL.

Stability in Simulated Gastrointestinal Fluids. Simulated gastric fluid (sGF) and simulated intestinal fluid (sIF) were prepared according to the United States Pharmacopeia (USP 28). sGF contained sodium chloride (200 mg), pepsin (320 mg), and 37% aq HCl (0.7 mL) in bidistilled water (100 mL). sIF consisted of monopotassium phosphate (680 mg), 0.2 M NaOH (7.7 mL), and pancreatin (1 g) in bidistilled water (100 mL). sIF was adjusted to pH 6 by adding 0.2 M NaOH. sGF and sIF were preheated (37 °C), and the compounds were added to yield 10 μ M solutions. Incubations were performed on a Eppendorf Thermomixer Comfort (500 rpm, 37 °C). Before starting the experiment ($t = 0$ min) and after an incubation time of 15, 30, 60, and 120 min, samples (20 μ L) were withdrawn, precipitated with ice-cooled MeCN, and centrifuged (3600 rpm, 4 °C, 10 min). The concentrations of analyte in the supernatant were analyzed by LC-MS. Stability was expressed as percentage remaining compound relative to the initial concentration.

In Vitro Metabolism: Ester Hydrolysis. Incubations were performed in a 96-well format on a Eppendorf Thermomixer Comfort. Each compound was incubated with a reaction mixture (270 μ L) consisting of pooled male mouse liver microsomes in the presence of TRIS buffer (0.1 M, pH 7.4) and MgCl₂ (2 mM). After preheating (37 °C, 500 rpm, 10 min), the incubation was initiated by adding 30 μ L of compound solution (20 μ M) in TRIS buffer. The final concentration of the compounds was 2 μ M, and the microsomal concentration was 0.25 mg/mL. At the beginning of the experiment ($t = 0$ min) and after an incubation time of 1, 3, 6, and 15 min, samples (50 μ L) were transferred to 150 μ L of ice-cooled MeCN, centrifuged (3600 rpm, 4 °C, 10 min), and 80 μ L of supernatant were transferred to a 96-well plate for LC-MS analysis. Metabolic degradation was assessed as percentage remaining compound versus incubation time. Control experiments were performed in parallel by preincubating the microsomes with the specific carboxylesterase inhibitor BNPP (1 mM) for 5 min before addition of the antagonists.

In Vitro Metabolism: Cytochrome P450-Mediated Metabolism. Incubations consisted of pooled male mouse liver microsomes (0.5 mg microsomal protein/mL), compounds (2 μ M), MgCl₂ (2 mM), and NADPH (1 mM) in a total volume of 300 μ L TRIS buffer (0.1 M, pH 7.4) and were performed in a 96-well plate on a Thermomixer Comfort. Compounds and microsomes were preincubated (37 °C, 700 rpm, 10 min) before NADPH was added. Samples (50 μ L) at $t = 0$ min and after an incubation time of 5, 10, 20, and 30 min were quenched with 150 μ L of ice-cooled acetonitrile, centrifuged (3600 rpm, 4 °C, 10 min), and 80 μ L of each supernatant were transferred to a 96-well plate for LC-MS analysis. Control experiments without NADPH were performed in parallel.

LC-MS Measurements. Analyses were performed using a 1100/1200 series HPLC system coupled to a 6410 triple quadrupole mass detector (Agilent Technologies, Inc., Santa Clara, CA, USA) equipped with electrospray ionization. The system was controlled with the Agilent MassHunter Workstation Data Acquisition software (version B.01.04). The column used was an Atlantis T3 C18 column (2.1 mm \times 50 mm) with a 3 μ m particle size (Waters Corp., Milford, MA, USA). The mobile phase consisted of two eluents: solvent A (H₂O, containing 0.1%

formic acid, v/v) and solvent B (acetonitrile, containing 0.1% formic acid, v/v), both delivered at 0.6 mL/min. The gradient was ramped from 95% A/5% B to 5% A/95% B over 1 min, and then held at 5% A/95% B for 0.1 min. The system was then brought back to 95% A/5% B, resulting in a total duration of 4 min. MS parameters such as fragmentor voltage, collision energy, polarity were optimized individually for each drug, and the molecular ion was followed for each compound in the multiple reaction monitoring mode. The concentrations of the analytes were quantified by the Agilent Mass Hunter Quantitative Analysis software (version B.01.04).

In Vivo Pharmacokinetic and Disease Model. Bacteria. The clinical *E. coli* isolate UTI89⁵⁵ (UTI89wt) were kindly provided by the group of Prof. Urs Jenal, Biocenter, University of Basel. Microorganisms were stored at -70 °C and before experiment incubated for 24 h under static conditions at 37 °C in 10 mL of Luria-Bertani broth (Becton, Dickinson and Company, Le Pont de Claix, France) using 50 mL tubes. Prior to each experiment, the microorganisms were washed twice and resuspended in phosphate buffered saline (PBS, Hospital Pharmacy at the University Hospital Basel, Switzerland). Bacterial concentrations were determined by plating serial 1:10 dilutions on blood agar, followed by colony counting with 20–200 colonies after overnight incubation at 37 °C.

Animals. Female C3H/HeN mice weighting between 19 and 25 g were obtained from Charles River (Sulzfeld, Germany) and were housed four to a cage. Mice were kept under specific-pathogen-free conditions in the Animal House of the Department of Biomedicine, University Hospital Basel, and animal experimentation guidelines according to the regulations of Swiss veterinary law were followed. After seven days of acclimatization, 9- to 10-week old mice were used for the PK and infection studies. During the studies, animals were allowed free access to chow and water. Three days before infection studies and during infection, 5% D-(+)-glucose (AppliChem, Baden-Dättwil, Switzerland) was added to the drinking water to increase the number of bacterial counts in the urine and kidneys.⁵⁷

Pharmacokinetic Studies. Single-dose pharmacokinetic studies were performed by iv and po application of the FimH antagonists at a concentration of 50 mg/kg followed by urine and plasma sampling. For iv application, the antagonists (**1**, **17a**, **17b**) were diluted in 100 μ L of PBS and injected into the tail vein. For po application, antagonist **1** was diluted in 200 μ L of PBS and antagonists **17b** and **16b** were first dissolved in DMSO (20 \times) and then slowly diluted to the final concentration (1 \times) in 1% Tween-80/PBS to obtain a suspension. Antagonists were applied iv by injection into the tail vein and po using a gavage followed by blood and urine sampling (10 μ L) after 6 min, 30 min, 1 h, 2 h, 4 h, 6 h, 8 h, and 24 h. Before analysis, proteins in blood and urine samples were precipitated using methanol (Acros Organics, Basel, Switzerland) and centrifuged for 11 min at 13000 rpm. The supernatant was transferred into a 96-well plate (0.5 mL, polypropylene, Agilent Technologies, Basel, Switzerland) and analyzed by LC-MS as described above.

UTI Mouse Model. Mice were infected as previously described.⁵⁷ In brief, before infection, all remaining urine was depleted from the bladder by gentle pressure on the abdomen. Mice were anesthetized with 2.5 vol% isoflurane/oxygen mixture (Attane, Minrad Inc., Buffalo, NY, USA) and placed on their back. Anesthetized mice were inoculated transurethrally with the bacterial suspension by use of a 2 cm polyethylene catheter (Intramedic polyethylene tubing, inner diameter 0.28 mm, outer diameter 0.61 mm, Beckton Dickinson, Allschwil, Switzerland), which was placed on a syringe (Hamilton Gastight Syringe 50 μ L, removable 30G needle, BGB Analytik AG, Boeckten, Switzerland). The catheter was gently inserted through the urethra until it reached the top of the bladder, followed by slow injection of 50 μ L of bacterial suspension at a concentration of approximately 10⁹ to 10¹⁰ CFU/mL.

Antagonist Treatment Studies. FimH antagonists were applied iv in 100 μ L of PBS into the tail vein or po as a suspension by the help

of a gavage, 10 min (**17a**, **17b**, **16b**) or 1 h before infection (**1**). Three h after the onset of infection, urine was collected by gentle pressure on the abdomen and then the mouse was sacrificed with CO₂. Organs were removed aseptically and homogenized in 1 mL of PBS by using a tissue lyser (Retsch, Haan, Germany). Serial dilutions of urine, bladder, and kidneys were plated on Levine Eosin Methylene Blue Agar plates (Beckton Dickinson, Le Pont de Claix, France). CFU counts were determined after overnight incubation at 37 °C and expressed as CFU/mL for the urine and CFU/bladder and CFU/2 kidneys for the organs.

Acknowledgment. We thank Professor Rudi Glockshuber (ETH Zürich, Switzerland) for gratefully providing the plasmid pNT-FimH used for the cloning of the FimH CRD and *E. coli* strain HM 125. We thank Dr. Manfred Kansy and Dr. Christoph Funk, F. Hoffmann-La Roche AG, Basel, Switzerland, for supporting us with their expertise when we established the PADMET platform, and to Prof. Angelo Vedani, University of Basel, Switzerland, for fruitful discussions on conformational issues. We further appreciate the support by Prof. Dr. med. Radek Skoda, Department of Biomedicine, University Hospital Basel, Switzerland, for giving us access to the animal facility and Prof. Niels Frimodt-Møller, Statens Serum Institut, Copenhagen, Denmark for the introduction to the in vivo model. We thank Prof G. Imanidis, FHNW, Muttenz, Switzerland, for providing the Caco-2 cells, and Dr. M. Schneider, Department of Pharmaceutical Sciences, University of Basel, Switzerland, for his help during the assay build-up. We are grateful to Prof. Urs Jenal, Biocenter of the University of Basel, Switzerland, for the clinical *E. coli* isolate UTI89 and the FimH knock out strain UTI89Δ*fimA-H*. Finally, we thank the Swiss National Science Foundation (project K-32K1-120904) for their financial support.

Supporting Information Available: ¹H NMR spectra and HPLC traces for the target compounds **16a–e**, **17a–c,e**, **21a,b**, and **22a,b** and experimental and spectroscopic details for compounds **6a–d**, **7a–d**, **14c–e**, **15c–e**, **16c–e**, **17c,e**, **19a,b**, **20a,b**, and **21a,b**. This material is available free of charge via the Internet at <http://pubs.acs.org>.

References

- (1) Fihn, S. D. Clinical practice. Acute uncomplicated urinary tract infection in women. *N. Engl. J. Med.* **2003**, *349*, 259–266.
- (2) Hooton, T. M. Recurrent urinary tract infection in women. *Int. J. Antimicrob. Agents* **2001**, *17*, 259–268.
- (3) Wiles, T. J.; Kulesus, R. R.; Mulvey, M. A. Origins and virulence mechanisms of uropathogenic *Escherichia coli*. *Exp. Mol. Pathol.* **2008**, *85*, 11–19.
- (4) Gouin, S. G.; Wellens, A.; Bouckaert, J.; Kovensky, J. Synthetic Multimeric Heptyl Mannosides as Potent Antiadhesives of Uropathogenic *Escherichia coli*. *ChemMedChem* **2009**, *4*, 749–755.
- (5) Rosen, D. A.; Hung, C. S.; Kline, K. A.; Hultgren, S. J. Streptozocin-induced diabetic mouse model of urinary tract infection. *Infect. Immun.* **2008**, *76*, 4290–4298.
- (6) Mulvey, M. A. Adhesion and entry of uropathogenic *Escherichia coli*. *Cell Microbiol.* **2002**, *4*, 257–271.
- (7) Capitani, G.; Eidam, O.; Glockshuber, R.; Grutter, M. G. Structural and functional insights into the assembly of type 1 pili from *Escherichia coli*. *Microbes Infect.* **2006**, *8*, 2284–2290.
- (8) Choudhury, D.; Thompson, A.; Stojanoff, V.; Langermann, S.; Pinkner, J.; Hultgren, S. J.; Knight, S. D. X-ray structure of the FimC–FimH chaperone–adhesin complex from uropathogenic *Escherichia coli*. *Science* **1999**, *285*, 1061–1066.
- (9) Bouckaert, J.; Berglund, J.; Schembri, M.; Genst, E. D.; Cools, L.; Wuhler, M.; Hung, C. S.; Pinkner, J.; Slättergard, R.; Zavialov, A.; Choudhury, D.; Langermann, S.; Hultgren, S. J.; Wyns, L.; Klemm, P.; Oscarson, S.; Knight, S. D.; Greve, H. D. Receptor binding studies disclose a novel class of high-affinity inhibitors of the *Escherichia coli* FimH adhesin. *Mol. Microbiol.* **2005**, *55*, 441–455.
- (10) Wellens, A.; Garofalo, C.; Nguyen, H.; Van Gerven, N.; Slättergard, R.; Hernalsteens, J.-P.; Wyns, L.; Oscarson, S.; De Greve, H.; Hultgren, S.; Bouckaert, J. Intervening with urinary tract infections using anti-adhesives based on the crystal structure of the FimH–oligomannose-3 complex. *PLoS ONE* **2008**, *3*, 4–13.
- (11) Langermann, S.; Mollby, R.; Burlein, J. E.; Palaszynski, S. R.; Auguste, C. G.; DeFusco, A.; Strouse, R.; Schenerman, M. A.; Hultgren, S. J.; Pinkner, J. S.; Winberg, J.; Guldevall, L.; Soderhall, M.; Ishikawa, K.; Normark, S.; Koenig, S. Vaccination with FimH adhesin protects cynomolgus monkeys from colonization and infection by uropathogenic *Escherichia coli*. *J. Infect. Dis.* **2000**, *181*, 774–778.
- (12) Langermann, S.; Palaszynski, S.; Barnhart, M.; Auguste, G.; Pinkner, J. S.; Burlein, J.; Barren, P.; Koenig, S.; Leath, S.; Jones, C. H.; Hultgren, S. J. Prevention of mucosal *Escherichia coli* infection by FimH-adhesin-based systemic vaccination. *Science* **1997**, *276*, 607–611.
- (13) Bouckaert, J.; Mackenzie, J.; de Paz, J. L.; Chipwaza, B.; Choudhury, D.; Zavialov, A.; Mannerstedt, K.; Anderson, J.; Pierard, D.; Wyns, L.; Seeberger, P. H.; Oscarson, S.; De Greve, H.; Knight, S. D. The affinity of the FimH fimbrial adhesin is receptor-driven and quasi-independent of *Escherichia coli* pathotypes. *Mol. Microbiol.* **2006**, *61*, 1556–1568.
- (14) Sharon, N. Carbohydrates as future anti-adhesion drugs for infectious diseases. *Biochim. Biophys. Acta* **2006**, *1760*, 527–537.
- (15) (a) Firon, N.; Ofek, I.; Sharon, N. Interaction of mannose-containing oligosaccharides with the fimbrial lectin of *Escherichia coli*. *Biochem. Biophys. Res. Commun.* **1982**, *105*, 1426–1432. (b) Firon, N.; Ofek, I.; Sharon, N. Carbohydrate specificity of the surface lectins of *Escherichia coli*, *Klebsiella pneumoniae* and *Salmonella typhimurium*. *Carbohydr. Res.* **1983**, *120*, 235–249. (c) Sharon, N. Bacterial lectins, cell–cell recognition and infectious disease. *FEBS Lett.* **1987**, *217*, 145–157.
- (16) (a) Neeser, J.-R.; Koellreutter, B.; Wuersch, P. Oligomannoside-type glycopeptides inhibiting adhesion of *Escherichia coli* strains mediated by type 1 pili: preparation of potent inhibitors from plant glycoproteins. *Infect. Immun.* **1986**, *52*, 428–436. (b) Lindhorst, T. K. Artificial multivalent sugar ligands to understand and manipulate carbohydrate–protein interactions. *Top. Curr. Chem.* **2002**, *218*, 201–235 (review); (c) Patel, A.; Lindhorst, T. K. A modular approach for the synthesis of oligosaccharide mimetics. *Carbohydr. Res.* **2006**, *341*, 1657–1668. (d) Nagahori, N.; Lee, R. T.; Nishimura, S.-L.; Pagé, S.; Roy, R.; Lee, Y. C. Inhibition of adhesion of type 1 fimbriated *Escherichia coli* to highly mannosylated ligands. *ChemBioChem* **2002**, *3*, 836–844. (e) Appeldoorn, C. C. M.; Joosten, J. A. F.; Maate, F. A.; Dobrindt, U.; Hacker, J.; Liskamp, R. M. J.; Khan, A. S.; Pieters, R. J. Novel multivalent mannose compounds and their inhibition of the adhesion of type 1 fimbriated uropathogenic *E. coli*. *Tetrahedron Asymmetry* **2005**, *16*, 361–372. (f) Touaibia, M.; Wellens, A.; Shiao, T. C.; Wang, Q.; Sirois, S.; Bouckaert, J.; Roy, R. Mannosylated G(0) dendrimers with nanomolar affinities to *Escherichia coli* FimH. *Chem-MedChem* **2007**, *2*, 1190–1201.
- (17) (a) Firon, N.; Ashkenazi, S.; Mirelman, D.; Ofek, I.; Sharon, N. Aromatic alpha-glycosides of mannose are powerful inhibitors of the adherence of type 1 fimbriated *Escherichia coli* to yeast and intestinal epithelial cells. *Infect. Immun.* **1987**, *55*, 472–476. (b) Lindhorst, T. K.; Kötter, S.; Kubisch, J.; Krallmann-Wenzel, U.; Ehlers, S.; Kren, V. Effect of p-substitution of aryl α-D-mannosides on inhibiting mannose-sensitive adhesion of *Escherichia coli*—synthesis and testing. *Eur. J. Org. Chem.* **1998**, 1669–1674. (c) Sperling, O.; Fuchs, A.; Lindhorst, T. K. Evaluation of the carbohydrate recognition domain of the bacterial adhesin FimH: design, synthesis and binding properties of mannose ligands. *Org. Biomol. Chem.* **2006**, *4*, 3913–3922. (d) Han, Z.; Pinker, J. S.; Ford, B.; Obermann, R.; Nolan, W.; Wildman, S. A.; Hobbs, D.; Ellenberger, T.; Cusumano, C. K.; Hultgren, S. J.; Janetka, J. W. Structure-Based Drug Design and Optimization of Mannoside Bacterial FimH Antagonists. *J. Med. Chem.* **2010**, *53*, 4779–4792. (e) Berglund, J.; Bouckaert, J.; De Greve, H.; Knight, S. Anti-adhesive compounds to prevent and treat bacterial infections. International Patent Application PCT/US 2005/089733, 2005.
- (18) Hung, C. S.; Bouckaert, J.; Hung, D.; Pinkner, J.; Widberg, C.; Defusco, A.; Auguste, C. G.; Strouse, R.; Langermann, S.; Waksman, G.; Hultgren, S. J. Structural basis of tropism of *Escherichia coli* to the bladder during urinary tract infection. *Mol. Microbiol.* **2002**, *44*, 903–918.
- (19) Ernst, B.; Magnani, J. L. From carbohydrate leads to glycomimetic drugs. *Nature Rev. Drug Discovery* **2009**, *8*, 661–677.
- (20) (a) Lindhorst, T. K.; Kieburg, C.; Krallmann-Wenzel, U. Inhibition of the type 1 fimbriae-mediated adhesion of *Escherichia coli* to erythrocytes by multiantennary α-mannosyl clusters: the effect of multivalency. *Glycoconjugate J.* **1998**, *15*, 605–613. (b) Dubber, M.; Sperling, O.; Lindhorst, T. K. Oligomannoside mimetics by glycosylation of 'octopus glycosides' and their investigation as inhibitors of type 1

- fimbriae-mediated adhesion of *Escherichia coli*. *Org. Biomol. Chem.* **2006**, *4*, 3901–3912. (c) Touaibia, M.; Wellens, A.; Shiao, T. C.; Wang, Q.; Sirois, S.; Bouckaert, J.; Roy, R. Mannosylated G0 dendrimers with nanomolar affinities to *Escherichia coli* FimH. *ChemMedChem* **2007**, *2*, 1190–1201.
- (21) Aronson, M.; Medalia, O.; Schori, L.; Mirelman, D.; Sharon, N.; Ofek, I. Prevention of colonization of the urinary tract of mice with *Escherichia coli* by blocking of bacterial adherence with methyl α -D-mannopyranoside. *J. Infect. Dis.* **1979**, *139*, 329–332.
- (22) Svanborg Eden, C.; Freter, R.; Hagberg, L.; Hull, R.; Leffer, H.; Schoolnik, G. Inhibition of experimental ascending urinary tract infection by an epithelial cell-surface receptor analog. *Nature* **1982**, *298*, 560–562.
- (23) Rabbani, S.; Jiang, X.; Schwardt, O.; Ernst, B. Expression of the carbohydrate recognition domain of FimH and development of a competitive binding assay. *Anal. Biochem.* **2010**, *407*, 188–195.
- (24) Ness, R. K.; Fletcher, H. G.; Hudson, C. S. Reaction of 2,3,4,6-tetrabenzoyl- α -D-glucopyranosyl bromide and 2,3,4,6-tetrabenzoyl- α -D-mannopyranosyl bromide with methanol. Certain benzoylated derivatives of D-glucose and D-mannose. *J. Am. Chem. Soc.* **1950**, *72*, 2200–2205.
- (25) Sancho-Garcia, J. C.; Cornil, J. Anchoring the Torsional Potential of Biphenyl at the ab Initio Level: The Role of Basis Set versus Correlation Effects. *J. Chem. Theory Comput.* **2005**, *1*, 581–589.
- (26) Eaton, V. J.; Steele, D. Dihedral angle of biphenyl in solution and the molecular force field. *J. Chem. Soc., Faraday Trans. 2* **1973**, 1601–1608.
- (27) Albert, A. Chemical aspects of selective toxicity. *Nature* **1958**, *182*, 421–422.
- (28) Winiwarter, S.; Bonham, N. M.; Ax, F.; Hallberg, A.; Lennernäs, H.; Karlén, A. Correlation of Human Jejunal Permeability (in Vivo) of Drugs with Experimentally and Theoretically Derived Parameters. A Multivariate Data Analysis Approach. *J. Med. Chem.* **1998**, *41*, 4939–4949.
- (29) Taketani, M.; Shii, M.; Ohura, K.; Ninomiya, S.; Imai, T. Carboxylesterase in the liver and small intestine of experimental animals and human. *Life Sci.* **2007**, *81*, 924–932.
- (30) Kansy, M.; Senner, F.; Gubernator, K. Physicochemical High Throughput Screening: Parallel Artificial Membrane Permeation Assay in the Description of Passive Absorption Processes. *J. Med. Chem.* **1998**, *41*, 1007–1010.
- (31) Artursson, P.; Karlsson, J. Correlation between oral drug absorption in humans and apparent drug permeability coefficients in human intestinal epithelial (Caco-2) cells. *Biochem. Biophys. Res. Com.* **1991**, *175*, 880–885.
- (32) Varma, M. V. S.; Feng, B.; Obach, R. S.; Troutman, M. D.; Chupka, J.; Miller, H. R.; El-Kattan, A. Physicochemical Determinants of Human Renal Clearance. *J. Med. Chem.* **2009**, *52*, 4844–4852.
- (33) Abgottspon, D.; Rölli, G.; Hosch, L.; Steinhuber, A.; Jiang, X.; Schwardt, O.; Cutting, B.; Smiesko, M.; Jenal, U.; Ernst, B.; Trampuz, A. Development of an Aggregation Assay to Screen FimH Antagonists. *J. Microbiol. Methods* **2010**, *82*, 249–255.
- (34) Zhou, G.; Mo, W.-J.; Sebbel, P.; Min, G.; Neubert, T. A.; Glockshuber, R.; Wu, X.-R.; Sun, T.-T.; Kong, X.-P. Uroplakin Ia is the urothelial receptor for uropathogenic *Escherichia coli*: evidence from in vitro FimH binding. *J. Cell Sci.* **2001**, *114*, 4095–4103.
- (35) (a) Kartha, K. P. R.; Field, R. A. Iodine: a versatile reagent in carbohydrate chemistry. IV. Per-O-acetylation, regioselective acylation and acetolysis. *Tetrahedron* **1997**, *53*, 11753–11766. (b) Chittaboina, S.; Hodges, B.; Wang, Q. A facile route for the regioselective deacetylation of peracetylated carbohydrates at anomeric position. *Lett. Org. Chem.* **2006**, *3*, 35–38. (c) Mori, M.; Ito, Y.; Ogawa, T. Total synthesis of the mollu-series glycosyl ceramides α -D-Manp-(1 \rightarrow 3)- β -D-Manp-(1 \rightarrow 4)- β -D-Glcp-(1 \rightarrow 1)-Cer and α -D-Manp-(1 \rightarrow 3)-[β -D-Xylp-(1 \rightarrow 2)]- β -D-Manp-(1 \rightarrow 4)- β -D-Glcp-(1 \rightarrow 1)-Cer. *Carbohydr. Res.* **1990**, *195*, 199–224. (d) Egusa, K.; Kusumoto, S.; Fukase, K. Solid-phase synthesis of a phytoalexin elicitor pentasaccharide using a 4-azido-3-chlorobenzyl group as the key for temporary protection and catch-and-release purification. *Eur. J. Org. Chem.* **2003**, 3435–3445.
- (36) Giampapa, C. S.; Abraham, S. N.; Chiang, T. M.; Beachey, E. H. Isolation and characterization of a receptor for type 1 fimbriae of *Escherichia coli* from guinea pig erythrocytes. *J. Biol. Chem.* **1988**, *263*, 5362–5367.
- (37) Aprikian, P.; Tchesnokova, V.; Kidd, B.; Yakovenko, O.; Yarov-Yarovoy, V.; Trinchina, E.; Vogel, V.; Thomas, W.; Sokurenko, E. Interdomain interaction in the FimH adhesin of *Escherichia coli* regulates the affinity to mannose. *J. Biol. Chem.* **2007**, *282*, 23437–23446.
- (38) Trong, I. L.; Aprikian, P.; Kidd, B. A.; Forero-Shelton, M.; Tchesnokova, V.; Rajagopal, P.; Rodriguez, V.; Interlandi, G.; Klevit, R.; Vogel, V.; Stenkamp, R. E.; Sokurenko, E. V.; Thomas, W. E. Structural basis for mechanical force regulation of the adhesin FimH via finger trap-like beta sheet twisting. *Cell* **2010**, *141*, 645–655.
- (39) Khoo, U. S.; Chan, K. Y. K.; Chan, V. S. F.; Lin, C. L. S. DC-SIGN and L-SIGN: the SIGNs for infection. *J. Mol. Med.* **2008**, *86*, 861–874.
- (40) Lee, S. J.; Evers, S.; Roeder, D.; Parlow, A. F.; Risteli, J.; Risteli, L.; Lee, Y. C.; Feizi, T.; Langen, H.; Nussenzweig, M. C. Mannose receptor-mediated regulation of serum glycoprotein homeostasis. *Science* **2002**, *295*, 1898–1901.
- (41) East, L.; Isacke, C. M. The mannose receptor family. *Biochim. Biophys. Acta* **2002**, *1572*, 364–386.
- (42) Dommett, R. M.; Klein, N.; Turner, M. W. Mannose-binding lectin in innate immunity: past, present and future. *Tissue Antigens* **2006**, *68*, 193–209.
- (43) Scharenberg, M. Expression and purification of DC-SIGN-CRD-Fc-IgG. Unpublished results.
- (44) Dearden, J. C.; Bresnen, J. G. M. The measurement of partition coefficients. *QSAR Comb. Sci.* **1988**, *7*, 133–144.
- (45) Wittwer, M.; Bezençon, J.; Cutting, B.; Wagner, B.; Kansy, M.; Ernst, B. pK_a determination by $^1\text{H-NMR}$ spectroscopy—an old methodology revisited. Unpublished results.
- (46) Banker, M. J.; Clark, T. H.; Williams, J. A. Development and validation of a 96-well equilibrium dialysis apparatus for measuring plasma protein binding. *J. Pharm. Sci.* **2003**, *92*, 967–974.
- (47) Kerns, E. H. High throughput physicochemical profiling for drug discovery. *J. Pharm. Sci.* **2001**, *90*, 1838–1858.
- (48) Avdeef, A.; Bendels, S.; Di, L.; Faller, B.; Kansy, M.; Sugano, K.; Yamauchi, Y. Parallel artificial membrane permeability assay (PAMPA)-critical factors for better predictions of absorption. *J. Pharm. Sci.* **2007**, *96*, 2893–2909.
- (49) Brandt, E.; Heymann, E.; Mentlein, R. Selective inhibition of rat liver carboxylesterases by various organophosphorus diesters in vivo and in vitro. *Biochem. Pharmacol.* **1980**, *29*, 1927–1931.
- (50) Scharenberg, M.; Abgottspon, D. Personal communication.
- (51) Obach, R. S. Prediction of human clearance of twenty-nine drugs from hepatic microsomal intrinsic clearance data: an examination of in vitro half-life approach and nonspecific binding to microsomes. *Drug Metab. Dispos.* **1999**, *27*, 1350–1359.
- (52) Trainor, G. L. The importance of plasma protein binding in drug discovery. *Expert Opin. Drug Discovery* **2007**, *2*, 51–64.
- (53) Weisiger, R. A. Dissociation from albumin: a potentially rate-limiting step in the clearance of substances by the liver. *Proc. Natl. Acad. Sci. U.S.A.* **1985**, *82*, 1563–1567.
- (54) Urien, S.; Tillement, J.-P.; Barre, J., The significance of plasma protein binding in drug research. In *Pharmacokinetic Optimization in Drug Research: Biological, Physicochemical, and Computational Strategies*; Wiley-VCH: Weinheim, Germany, 2001; pp 189–197.
- (55) Mulvey, M. A.; Schilling, J. D.; Hultgren, S. J. Establishment of a persistent *Escherichia coli* reservoir during the acute phase of a bladder infection. *Infect. Immun.* **2001**, *69*, 4572–4579.
- (56) (a) VCCLAB, Virtual Computational Chemistry Laboratory; <http://www.vcclab.org>, 2005; (b) Tetko, I. V.; Gasteiger, J.; Todeschini, R.; Mauri, A.; Livingstone, D.; Ertl, P.; Palyulin, V. A.; Radchenko, E. V.; Zefirov, N. S.; Makarenko, A. S.; Tanchuk, V. Y.; Prokopenko, V. V. Virtual computational chemistry laboratory—design and description. *J. Comput.-Aided Mol. Des.* **2005**, *19*, 453–463.
- (57) Kerr, M. B.; Frimodt-Møller, N.; Espersen, F. Effects of Sulfo-methizole and Amdinocillin against *Escherichia coli* Strains (with Various Susceptibilities) in an Ascending Urinary Tract Infection Model. *Antimicrob. Agents Chemother.* **2003**, *47*, 1002–1009.